INVESTIGATION OF LONG PERIOD NOISE AT LASA

Jack Capon

Massachusetts Institute of Technology
Lexington, Massachusetts

3 June 1968

INVESTIGATION OF LONG PERIOD NOISE
AT LASA

JACK CAPON

Group 64

ABSTRACT

The long-period noise in the 20 to 40 second period range limits the identification level at which the surface-wave, body-wave discriminant can be applied at the Large Aperture Seismic Array (LASA). Therefore, an investigation was made to determine the sources and properties of this noise. Only the long-period vertical array at LASA was considered.

Both conventional and high-resolution frequency-wavenumber spectra are presented for the noise, as well as coherence results. These data show that the noise consists of two components. One component propagates across the array as fundamental-mode Rayleigh waves and is known to be caused by the action of surf on coastlines. The other component is nonpropagating and evidence is presented which indicates it is caused by the elastic loading on the ground by the earth's atmosphere. This is established by correlating the power of the nonpropagating noise with the power on the micro-barograph sensors at LASA.

It is also shown that the signal-to-noise ratio gain obtained with maximum-likelihood processing relative to that obtained with beamforming for the long-period noise present at LASA, will not be substantial unless it can be shown that significant amounts of propagating noise power, relative to total noise power, are present. The results at LASA indicate that such large amounts of propagating noise power are rarely to be observed.

I. INTRODUCTION

The Large Aperture Seismic Array (LASA) located in eastern Montana consists of 21 subarrays of 25 short-period (SP) vertical seismometers as indicated in Fig. 1. At the center of each subarray there is a three-component set of long-period (LP) seismometers oriented in the vertical (Z), north-south (NS), and east-west (EW) directions. The primary function of LASA is to provide data for facilitating the discrimination between earthquakes and underground nuclear detonations.

It has been found that a useful discriminant for distinguishing between natural seismic events and underground nuclear explosions is based on the relationship between the surface-wave magnitude (M_s) and the body-wave magnitude (m_b).[1-5] The surface-wave magnitude M_s is based on the amplitude of Rayleigh waves with periods of about 20 seconds and is computed as[6]

$$M_s = \log A - \log B$$

where A is the ground amplitude of Rayleigh waves, in millimicrons, with periods of about 20 seconds recorded on LPZ seismometers, $-\log B$ is a parameter which depends on epicentral distance and is given by

$$-\log B = 1.656 \log (\Delta) - 1.182$$

where Δ is epicentral distance in degrees. The body-wave magnitude m_b is based on the amplitude of SP waves recorded at teleseismic distances and is computed according to the formula[7]

$$m_b = \log(w/T) + Q$$

where w is the maximum zero-to-peak ground amplitude, in millimicrons, of the first three to four cycles of the P-wave recorded on vertical component SP seismometers, T is the period, in seconds, of the observed short-period cycle and Q is a parameter which depends on epicentral distance and focal depth and is tabulated in Fig. 5 of Reference 7.

An experiment was performed to determine the effectiveness of a single LASA in using the $M_s - m_b$ discriminant at teleseismic distances and the results have been given recently.[8] The results of this experiment were very encouraging since a perfect separation was found to exist between the $M_s - m_b$ characteristic for earthquakes from four tectonic regions of the earth and that for presumed underground nuclear explosions from the Central Asian region. These results indicate that if the Rayleigh wave of an event can be detected along with the P-wave, then it is possible to distinguish whether the source is an earthquake or underground nuclear explosion with very little, if any, error.

Unfortunately, the Rayleigh wave of an event is not as readily detectable as the P-wave of the event. That is to say, the signal-to-noise ratio for the P-wave on the

2

vertical-component SP seismometer, at about 1 Hz, is usually considerably better than that for the Rayleigh wave on the vertical-component LP seismometer at 0.04 Hz. The signal-to-noise ratio gain provided by LASA for the P-wave by means of beamforming is about 20 db. Similarly, the signal-to-noise ratio gain provided by LASA for the Rayleigh wave by means of beamforming is about 11 db, and there is an additional 8 db gain from matched filtering, for a total of about 19 db. Thus, the signal-to-noise ratio of the processed P-wave is still considerably better than that of the processed Rayleigh wave. In other words, after all of the signal processing available at LASA has been performed, it is easier to detect the P-wave above the background noise level than it is to detect the Rayleigh wave. In this sense, it is the background LP noise level in the 20 to 40 second period range which is limiting the identification level at which the powerful $M_s - m_b$ discriminant can be applied. It is for this reason that a detailed investigation of the nature of the background LP noise was made in the 20 to 40 second period signal band.

It was found that the noise level on the EW and NS LP seismometers at LASA was usually about 10 db higher than the Z component.[8] It is for this reason that only the Z components were considered. This also tends to simplify the interpretation of the data and reduces the amount of data processing required.

The amount of noise introduced by the LP system was also determined. It was found that the LP system contributes a negligible amount of noise power.

The LP noise was analyzed by measuring its frequency-wavenumber spectrum with both conventional and high-resolution frequency-wavenumber measurement programs. A detailed description of these programs is given in Appendix A and B. These results indicate that the noise can be considered as composed of two components, a component which propagates across the LASA and a nonpropagating component which is found to be incoherent over spatial lags greater than 7.5 km. The propagating component of the LP noise, in the 20 to 40 second period range, is known to be caused by the action of surf on coastlines.[9] However, the source of the nonpropagating component of the noise is not nearly as well established. In the present work considerable evidence will be presented to indicate that the nonpropagating component of the noise is caused by the elastic loading on the earth by the atmosphere. This result was obtained by utilizing the microbarograph sensors available at LASA.

As a consequence of the preceding results, the frequency-wavenumber structure of the noise can be determined quite accurately. Using this structure it is possible to predict the processing gains to be expected by a multichannel filtering method such as the maximum-likelihood method. These processing gains are computed and presented subsequently and are shown to agree with the results obtained previously by processing actual LP noise data, cf. Reference 8.

II.   NOISE INTRODUCED BY LONG-PERIOD SYSTEM

The first step in the investigation of LP noise at LASA was to determine how much noise was introduced by the LP system shown in Fig. 2. In this section both the EW and NS components were considered as well as the Z component. The transfer function of the LP system is shown in Fig. 3. In order to determine the amount of noise introduced by the LP system the seismometer mass was locked on the EW, NS, Z components at site D2. The spectra of these components, as well as those at sites C2 and D1, were measured and the results are shown in Fig. 4. The frequency resolution used in this measurement was 0.013 Hz and a Hanning window was employed.[10] It is seen from Fig. 4 that the noise introduced by the LP system, as given in the spectra for site D2, is about 10 to 30 db lower than that of sites C2, D1 in the 0.025 to 0.05 Hz LP signal frequency band. Since these latter two sites can be considered as having an average noise level, we may conclude that the noise introduced by the LP system is negligible.

A similar test was conducted to determine how much of the LP system noise is due to the LP system exclusive of the LP seismometer. Towards this end the EW, NS, Z seismometers at site D2 were replaced with a 50 K resistance. The spectra of all three components at site D2 were measured in the manner just described, and are shown in Fig. 5 along with the results for sites C2 and D1. The spectrum for the EW component at site C2 is anomalously low due to anomalous signal on this seismometer at the time. It is observed from Fig. 5 that the noise levels at site D2 are comparable to

5

those obtained during the locked mass test, as seen in Fig. 4. Therefore, it may be concluded that most of the noise introduced by the LP system is due to the LP system exclusive of the seismometer.

III.   FREQUENCY-WAVENUMBER STRUCTURE OF LONG-PERIOD NOISE

The frequency-wavenumber spectrum of the LP seismic noise provides the information about the distribution of noise power with frequency and for a fixed frequency reveals the velocity and direction of propagation of the noise, cf. reference 11 and Appendix A. Both conventional and high-resolution frequency-wavenumber spectra of the LP seismic noise were measured. The method of measurement is discussed in detail in Appendix A and B. The conventional frequency-wavenumber spectrum measurement program is due to R. T. Lacoss.[12] As mentioned previously, only the Z components of the array will be considered. All of the sensors at LASA were used to measure the frequency-wavenumber spectrum except for those sensors which yielded anomalous traces. The frequency resolution employed was 0.01 Hz, a Bartlett window[10] was used, and a direct segment, or block averaging, method was employed with the averaging performed over 36 blocks. This leads to 72 degrees of freedom or 90% confidence limits of about $\pm$ 1.2 db.[10] The sampling rate of the data is 5 Hz but a decimation factor of 5 was employed so that a sampling rate of 1 Hz was used in the measurement. The total length of data employed in the measurement was one hour.

The results of both the conventional and high-resolution frequency-wavenumber programs are shown in Figs. 6-8 for three different noise samples taken on 26 February 1967, 7 April 1967 and 26 January 1967, respectively, and for three frequencies, 0.03, 0.04 and 0.05 Hz. These figures show that the conventional and high-resolution results are in agreement as both methods tend to show strong peaks occurring at the same

wavenumber in each progr . . However, the high-resolution method delineates the frequency-wavenumber spectrum much more clearly than the conventional method. This is demonstrated quite well in Fig. 6c, which shows the wavenumber structure of the propagating noise to be an arc. This is, of course, exactly what would be expected, since the dispersion curve of the propagating seismic noise at LASA has been measured and found to correspond to that of a fundamental mode Rayleigh wave. [12] This implies that at a given period the phase velocity of the propagating noise at LASA must be constant, independent of the sources of the noise, and thus its wavenumber structure must consist of an arc, or arcs, whose extent corresponds to the range of the azimuths of the noise sources.

An interesting example is provided by the 26 January 1967 noise sample, for which the results are given in Fig. 8. In particular, Fig. 8c shows a 360 degree azimuthal spread for the wavenumber structure with a variable energy density along this circle.

The preceding results show that the LPZ seismic noise consists of two components, a component which is propagating across the array as fundamental mode Rayleigh waves and a component which is nonpropagating or incoherent. The nonpropagating component has been found to be incoherent over distances greater than 7.5 km, by measuring the coherence between LPZ sensors during time periods when the propagating noise was absent and noting that the coherence was down to the level corresponding to incoherent noise. A description of this coherence measurement program is given in Appendix A.

8

A simulation was performed by computing conventional and high-resolution frequency wavenumber spectra for theoretical models of the noise which correspond to the preceding description of the noise. These simulation results were in excellent agreement with those obtained for the actual noise data.

It is quite important to know the relative amounts of the two kinds of noise. Towards this end, the coherence was measured for spatial lags between 7.5 and 20 km. Since the wavelengths of the propagating noise are on the order of 75 to 90 km, these lags correspond to a small fraction of a wavelength and this component of the noise can be considered to be perfectly coherent over these spatial lags. Hence, any measured loss of coherence over these small spatial lags must be due to the nonpropagating component of the LPZ noise. The relative amount of power in the propagating component, relative to the total power was obtained by averaging together the coherencies measured over the small spatial lags. In addition, the bias introduced in the measurement was taken into account by using the tables of Amos and Koopmans[13] with their degrees of freedom parameter set equal to the number of blocks used in the coherence measurement, cf. Fig. 9. It is tacitly assumed that the noise power is the same in each LPZ sensor. This is not actually true, but is a good approximation since the noise power in any sensor does not usually vary from the average noise power taken over all of LASA by about 2 − 3 db.

The relative amounts of noise power were measured in this manner at 0.03, 0.04, and 0.05 Hz and the results were then summed over these frequencies to obtain

an approximation for the total and relative amounts of noise power in the 0.025 to 0.05 Hz LP signal band. The results for the total power in this band were checked independently for two noise samples by prefiltering the data with a sharp cutoff 400 second bandpass convolutional filter, 0.025 to 0.05 Hz, and then measuring the noise power by summing the squares of the noise samples. The two methods gave results which were in agreement within 1.5 db. The results of this experiment are shown in Fig. 10 for 31 noise samples extending in time over a period of about 14 months. The results of Fig. 10 show that there is a considerable spread in the total LPZ noise power, of about 12 db. This means that the identification threshold at LASA, using the $M_s - m_b$ discriminant, will be variable depending on the amount of background noise power that is present.

A cumulative probability distribution was measured for the ratio of nonpropagating to total noise power and the results are shown in Fig. 11. It is seen from this figure that 50 percent of the time this ratio is greater than 0.4. This fact has important implications in the consideration of array processing methods for obtaining signal-to-noise ratio gain, as will be seen subsequently.

A histogram of noise-source azimuths observed at LASA was measured at the 25 second period for the 31 noise samples mentioned previously, using the measured frequency-wavenumber spectra. This histogram is shown in Fig. 12. It is observed that much of the time the propagating noise tends to come from the northwest and northeast directions.

10

IV. COHERENCE BETWEEN LONG-PERIOD SEISMIC NOISE AND MICROBAROGRAPH SENSORS

It is important to establish the origin of the nonpropagating LPZ seismic noise. Previous results due to Haubrich and MacKenzie[9] indicate that this noise might be due to the elastic loading on the earth by the atmosphere. Thus, an effort was made to determine the coherence between the LPZ seismic noise and the atmospheric fluctuations as recorded on microbarograph sensors at LASA.

The LP seismometers are located in sealed metal tanks embedded in the floor of an underground concrete structure, known as the LP vault. Each tank is sealed and tested for a leakage rate time constant of at least eight hours. Thus, any atmospheric buoyancy effects on the mass of the LP seismometer, in the 20 to 40 second period range, have been effectively eliminated.

At the time of the present experiment there were five microbarograph installations at LASA, each located near the center of a subarray and usually less than a few hundred feet from the LP seismometers. In some cases, such as sites E3, B1 and B4 the microbarograph was actually located in the same vault as the LP seismometers. The characteristics of the microbarographs are given in Table I. The difference between the two microbarographs at site A0 is that one of them had various types of wind filters while the other used a single type of wind filter, namely a linear pipe array with orifices spaced 10 feet apart. Comparable results were obtained with either of these two microbarographs.

The direct segment, or block averaging, method described in Appendix A was used to measure the coherence between LP seismometers and the microbarographs and also to measure the spectra of these sensors. The frequency resolution, frequency window,

11

TABLE I

CHARACTERISTICS OF MICROBAROGRAPHS

SITE	3 db RESPONSE PERIODS (SECONDS)	PHYSICAL LOCATION	TIME CONSTANT OF WIND FILTER (SECONDS)
A∅	10-60	CENTRAL TELEMETRY HOUSING	10
A∅	10-60	CENTRAL TELEMETRY HOUSING	10
B1	10-80	LP VAULT	10
B4	10-80	LP VAULT	10
E3	10-60U	LP VAULT	10

number of blocks, and decimation factor are the same as that used previously in Section III in the measurement of frequency-wavenumber spectra.

Typical spectra for the LPZ sensor at site A∅ and one of the microbarographs at site A∅ are shown in Fig. 13. The dates and times of the noise samples used to measure the coherence are listed in Table II. It should be noted that only 9 of the 17 noise samples showed any coherence between an LPZ seismometer at any site and its corresponding microbarograph. It is also worth noting that the noise samples were picked so as to have a reasonably large amount of nonpropagating noise in the 20 to 40 second period range. Two examples in which coherence was measured at site A∅ are given in Figs. 14a and b, where the latter figure is more typical of the behavior of the coherence when any coherence is measured at all. In Fig. 14a the coherence at 0.03 Hz is quite high, about 0.6 and drops to about 0.5 and 0.4 at 0.04 and 0.05 Hz, respectively. The ratio of nonpropagating noise to the total noise, for this noise sample, was measured as 0.9 at 0.03, 0.04 and 0.05 Hz. The measured coherence is not as high as this at these frequencies, but is the largest that was ever measured in all of the 17 noise samples. The results of Fig. 14b are more typical in that whenever coherence is measured, it tends to be high at 0.02 Hz and then drops to the level for incoherent noise at 0.03 to 0.05 Hz. The 95 percent confidence limits for this level for incoherent noise can be obtained from Fig. 9 as 0.02 to 0.3. The ratio of nonpropagating to total noise for the noise sample used in Fig. 14b was measured as 0.60, 0.45, and 0.35 at 0.03, 0.04 and 0.05 Hz, respectively. It is seen that the coherence never reaches a level compatible with the amount of nonpropagating noise. Thus, we may conclude that there is relatively little coherence between the LPZ noise and the microbarograph signals in the 20 to 40 second period range.

13

TABLE II

NOISE SAMPLES USED TO DETERMINE COHERENCE BETWEEN LPZ SEISMOMETERS AND MICROBAROGRAPHS

DATE	START TIME (GMT)
28 May 67*	03:40:00
3 June 67*	10:47:00
1 July 67*	19:50:00
10 July 67*	02:30:00
15 July 67*	02:50:00
29 July 67*	07:52:00
23 Aug 67*	17:20:00
2 Sept 67	01:43:00
30 Sept 67*	01:12:00
1 Oct 67	00:33:00
1 Nov 67	13:53:00
24 Nov 67	16:25:00
31 Dec 67*	04:05:00
5 Jan 68*	15:30:00
5 Jan 68	23:30:00
6 Jan 68	19:30:00
7 Jan 68	04:45:00

* Denotes that coherence was observed between LPZ seismometer and microbarograph.

EACH NOISE SAMPLE IS ONE HOUR LONG.

An attempt was made to correlate the amount of nonpropagating LPZ seismic noise power and the amount of microbarograph noise power in the 20 to 40 second period range. These quantities were measured at site A∅ for the 17 noise samples given in Table II and the results are shown in Fig. 15. This figure shows that there is a definite trend for the power level on the LPZ seismometer to increase when the power level on the microbarograph increases. Thus, this is evidence that the nonpropagating LPZ noise is caused by the elastic loading on the earth by the atmosphere. The non-propagating seismic noise may be caused by the cumulative effects of many independent atmospheric pressure fluctuation cells within a radius of a few km of the LPZ sensor and this may be the reason for the low coherence between this noise waveform and a single microbarograph record obtained at the same location.

V. COMPUTATION OF ARRAY PROCESSING GAIN FOR THEORETICAL MODEL OF SIGNAL AND NOISE

As a consequence of our preceding results it is possible to give a rather good representation for the structure of the LPZ seismic noise, in the 20 to 40 second period range, in frequency-wavenumber space. It has been established that the noise consists of two components. One component is propagating across the LASA as a fundamental-mode Rayleigh wave and its wavenumber structure, at a particular frequency, consists of an arc, or possibly, arcs. The radius of the arc, k, determines the phase velocity of the noise, v, by means of the equation $v = f/k$, where f is the frequency. The angular extent of the arc, or arcs, is determined by the azimuthal distribution of the noise. The other component of the noise is nonpropagating and incoherent and its coherence structure consists of a Kronecker delta function, i.e., the coherence is some value, between zero and unity, for zero spatial lag and is zero otherwise.

It is important to predict the signal-to-noise ratio gain achievable by various forms of array processing. If the wavenumber structure of the noise is known, at a given frequency, then for a fixed seismic array geometry it is possible to compute the signal-to-noise ratio gain of a particular form of array processing. This computation was performed using the array at LASA formed from the A, C, D, E and F rings, and the details of the computation are presented in Appendix C. The array processing methods considered were the maximum-likelihood and delay-and-sum, or beamforming, methods, cf. reference 14. The results of the computation are shown in Fig. 16 which

16

plots the gain of maximum-likelihood relative to beamforming vs azimuth of the noise

source and the extent of the arc. The wavenumber structure of the noise is assumed

to consist of a single arc and the azimuth of the noise source is defined as the azimuth

to the center of this arc. The array is assumed to be steered for an event from due

north whose phase velocity is 3.7 km/sec, the frequency is 0.04 Hz and the phase

velocity of the noise is also 3.7 km/sec. Results for other event steering parameters

yielded comparable results. The ratio of incoherent to total noise power, R, is 0.1,

0.3 and 0.5 in Figs. 16a, b, and c, respectively. These results show that when R = 0.1

there is significant gain of maximum-likelihood relative to beamforming, for a wide

range of noise source azimuths and arc extents. However, the condition R = 0.1 is

rarely met at LASA as can be seen from Fig. 11. The results in Figs. 16b and c show

that there is not much gain for maximum-likelihood relative to beamforming. These

conditions, when R = 0.3, 0.5, are more typical of the situation encountered at LASA.

It should be mentioned that these theoretical results were checked with results obtained

with actual data with reasonable agreement to within 2 db. The B-ring was omitted from

the computations since the effect of including it would have been to lower the gain of

beamforming considerably and increase the gain of maximum-likelihood only slightly,

due to the small diameter of the B-ring. When the B-ring is omitted, the amplitude

gain of beamforming is approximately equal to $\sqrt{NS}$, where NS is the number of sensors

in the array, provided the azimuth of the propagating noise is not within a half beamwidth

of the azimuth of the event. Note that NS = 21 − 4 = 17, $\sqrt{NS}$ = 5.4, which corresponds

17

to 12.3 db of gain. This aids in providing an approximate absolute scale for the gain of maximum-likelihood and beamforming methods when using the results of Fig. 16.

Thus, unless it can be established that significant amounts of noise are propagating as a fundamental-mode Rayleigh wave, the form of array processing to use is beamforming, because of its simplicity of implementation. The maximum-likelihood method is much more complicated and does not provide significant gain over beamforming unless $R < 0.3$, a condition which is rarely met at LASA. However, if it were possible to reduce the amount of nonpropagating noise, then the maximum-likelihood method would be very useful in obtaining large signal-to-noise ratio gains.

VI. CONCLUSIONS

The LPZ background seismic noise is limiting the identification threshold at which the $M_s - m_b$ discriminant can be applied. This noise has been investigated and found to consist of two components. One component propagates across LASA as a fundamental-mode Rayleigh wave, and is caused by the action of surf on coastlines. The other component is nonpropagating, or incoherent noise, and data have been obtained which indicate that it is caused by the elastic loading on the ground by the earth's atmosphere. This component always provides a significant contribution to the total noise power. As a consequence, it has been shown that sophisticated array processing methods such as maximum-likelihood cannot provide significant gain relative to beam-forming.

If the nonpropagating noise is caused by the action of the atmosphere on the ground, then the amplitude of this noise will be determined by the Lamé parameters of the medium, cf. reference 9, p. 1440. The LASA is located on sedimentary layers in eastern Montana, so that the Lamé parameters are relatively small. It is, therefore, desirable to construct any future array on granite whose Lamé parameters will be larger than those for sediments. This will lead to a reduction of the power of the non-propagating component of noise. In this case there may be an important role to be played by sophisticated array processing methods such as maximum-likelihood.

APPENDIX A

DESCRIPTION OF CONVENTIONAL FREQUENCY-WAVENUMBER
SPECTRUM MEASUREMENT PROGRAM

We assume that the noise $\{N_{jm}\}$, $j = 1, \ldots, K$, K is the number of sensors, is
a wide-sense stationary discrete-time parameter random process. The covariance
matrix of the noise is given by

$$\rho_{jk}(m-n) = E\{N_{jm} N_{km}\}, \quad j,k = 1, \ldots, K \tag{1}$$

where E denotes expectation. The cross-power spectral density is

$$f_{jk}(\lambda) = \sum_{m=-\infty}^{\infty} \rho_{jk}(m) \epsilon^{im\lambda}, \quad j,k = 1, \ldots, K \tag{2}$$

and

$$\rho_{jk}(m) = \int_{-\pi}^{\pi} f_{jk}(\lambda) \epsilon^{-im\lambda} \frac{d\lambda}{2\pi}, \tag{3}$$

where $\lambda = 2\pi fT$, f is frequency in Hz and T is the sampling period of the data in seconds.

If the noise field is space stationary, then, for fixed λ, $f_{j\ell}(\lambda)$ depends only on the
vector difference $\underline{x}_j - \underline{x}_\ell$, where $\underline{x}_j$ is the vector position of the jth sensor. It is con-
venient to introduce a cross-power spectral density $f(\lambda, \underline{r})$ as

20

$$f(\lambda, \underline{r}) = f_{j\ell}(\lambda), \quad \text{if } \underline{x}_j - \underline{x}_\ell = \underline{r}$$

and is also defined for all possible vector lags $\underline{r}$ in a similar manner. That is, we can imagine that sensors have been placed at any desired positions so that we can define $f(\lambda, \underline{r})$ as given above. It is now possible to define the frequency-wavenumber spectrum of the noise as

$$P(\lambda, \underline{k}) = \int_{-\infty}^{\infty} \int_{-\infty}^{\infty} f(\lambda, \underline{r}) \; \epsilon^{i\underline{k} \cdot \underline{r}} \; dr_x \, dr_y \tag{4}$$

where $\underline{k}$ is the vector wavenumber and r_x, r_y are the x, y components, respectively, of the vector $\underline{r}$. We may now use Eq. (4) to obtain $f_{j\ell}(\lambda)$ as

$$f_{j\ell}(\lambda) = \int_{-\infty}^{\infty} \int_{-\infty}^{\infty} P(\lambda, \underline{k}) \; \epsilon^{-i\underline{k} \cdot (\underline{x}_j - \underline{x}_\ell)} \; dk_x \, dk_y \qquad j, \ell = 1, \ldots, K \tag{5}$$

where k_x, k_y are the x, y components, respectively, of the vector $\underline{k}$, in radians/km.

If the noise consists of a unity amplitude monochromatic plane wave propagating with a velocity v_0, of the form $\epsilon^{i(2\pi f_0 jT - \underline{k}_0 \cdot \underline{r})}$, $j = 0, \pm 1, \pm 2, \ldots$, where f_0 is the frequency, $\underline{k}_0 = 2\pi f_0 \underline{\alpha}_0$, $\underline{\alpha}_0$ is a slowness vector which points in the direction of propagation of the wave and $|\underline{\alpha}_0| = 1/v_0$, then

$$f(\lambda, \underline{r}) = \epsilon^{-i\underline{k}_0 \cdot \underline{r}}$$

and

$$P(\lambda, \underline{k}) = \int\limits_{-\infty}^{\infty} \int\limits_{-\infty}^{\infty} \epsilon^{i(\underline{k}-\underline{k}_0) \cdot \underline{r}} \; dr_x \, dr_y$$

$$= \delta(\underline{k} - \underline{k}_0)$$

which is a delta function located at the wavenumber $\underline{k}_0$. It should now be apparent how $P(\lambda, \underline{k})$ provides the information concerning the speed and azimuth of propagating seismic waves.

The program which provides an estimate for $P(\lambda, \underline{k})$ employs the direct segment, or block averaging, method for reasons of computational efficiency, as described in reference 14. The number of data points, L, in each channel is divided into M non-overlapping blocks of N data points. The Fourier transform of the noise data in the nth segment, j^{th} channel, and normalized frequency λ, is

$$S_{jn}(\lambda) = (N)^{-1/2} \sum_{m=1}^{N} N_{j, m+(n-1)N} \, \epsilon^{im\lambda} \tag{6}$$

$$j = 1, \ldots, K$$
$$n = 1, \ldots, M.$$

As an estimate for $f_{jk}(\lambda)$ we take

$$\hat{f}_{jk}(\lambda) = \frac{1}{M} \sum_{n=1}^{M} S_{jn}(\lambda) \, S_{kn}^{*}(\lambda) \, , \qquad\qquad j, k = 1, \ldots, K \, . \tag{7}$$

At this point the program performs a normalization by dividing $\hat{f}_{jk}(\lambda)$ by $[\hat{f}_{jj}(\lambda) \hat{f}_{kk}(\lambda)]^{1/2}$, in order to remove the effects of improper sensor equalization. We can, without any loss of generality, ignore this step in the ensuing analysis.

22

As an estimate for $P(\lambda, \underline{k})$ we take

$$\hat{P}(\lambda, \underline{k}) = \frac{1}{K^2} \sum_{j,\ell=1}^{K} \hat{f}_{j\ell}(\lambda) \, \epsilon^{i\underline{k} \cdot (\underline{x}_j - \underline{x}_\ell)} \tag{8}$$

It was shown in reference 14 that $\{\hat{f}_{j\ell}(\lambda)\}$ is a nonnegative-definite matrix so that $\hat{P}(\lambda, \underline{k})$ will be real and nonnegative. Using the result in reference 14 for $E(\hat{f}_{j\ell}(\lambda))$ we get

$$E\{\hat{P}(\lambda, \underline{k}_0)\} = \int_{-\pi}^{\pi} \int_{-\infty}^{\infty} \int_{-\infty}^{\infty} P(\lambda, \underline{k}) \, |B(\underline{k} - \underline{k}_0)|^2 \, |W_N(x - \lambda)|^2 \, \frac{dx}{2\pi} \, dk_x \, dk_y \tag{9}$$

where $|W_N(x)|^2$ is the Bartlett window[10]

$$|W_N(x)|^2 = \frac{1}{N} \left| \frac{\sin (N/2) \, x}{\sin (1/2) \, x} \right|^2 \quad , \tag{10}$$

and $|B(\underline{k})|^2$ is the beamforming array response pattern

$$B(\underline{k}) = \frac{1}{K} \sum_{j=1}^{K} \epsilon^{i\underline{k} \cdot \underline{x}_j} \quad . \tag{11}$$

Thus, $E\{\hat{P}(\lambda, \underline{k}_0)\}$ is obtained by means of a frequency-wavenumber window $|W_N(x-\lambda)|^2 \, |B(\underline{k} - \underline{k}_0)|^2$. Hence, $\hat{P}$ will be an asymptotically unbiased estimate for cP if $|W_N(x - \lambda) \cdot B(\underline{k} - \underline{k}_0)|^2$ approaches a delta function in such a way that

$$\int_{-\pi}^{\pi} \int_{-\infty}^{\infty} \int_{-\infty}^{\infty} |W_N(x - \lambda) \cdot B(\underline{k} - \underline{k}_0)|^2 \, \frac{dx}{2\pi} \, dk_x \, dk_y = c$$

23

where c is some positive constant. The beamforming array response pattern for the LPZ array at LASA is given in Fig. 17 which shows $-20 \log |B(\underline{k})|$ $\underline{vs}$ $\frac{k_x}{2\pi}$, $\frac{k_y}{2\pi}$, in cycles/km.

Using the results of reference 14 we can compute the variance of $\hat{P}$ as, assuming $\{N_{jm}\}$ is a multidimensional Gaussian process,

$$\text{VAR}[\hat{P}(\lambda,\underline{k}_0)] = \frac{1}{M} \{E[\hat{P}(\lambda,\underline{k}_0)]\}^2 + \frac{1}{M} \left| \int_{-\pi}^{\pi} \int_{-\infty}^{\infty} \int_{-\infty}^{\infty} P(\lambda,\underline{k}) B^*(\underline{k}-\underline{k}_0) B(\underline{k}+\underline{k}_0) \cdot \right.$$

$$\left. \cdot |W_N(x-\lambda)|^2 \frac{dx}{2\pi} dk_x dk_y \right|^2$$

Thus

$$\text{VAR}[\hat{P}(\lambda,\underline{k}_0)] \simeq \frac{1}{M} \{E[\hat{P}(\lambda,\underline{k}_0)]\}^2, \qquad |\underline{k}_0| \neq 0$$

$$= \frac{2}{M} \{E[\hat{P}(\lambda,\underline{k}_0)]\}^2, \qquad |\underline{k}_0| = 0. \tag{12}$$

The mean and variance of $\hat{P}$ are given by Eqs. (9) and (12), respectively.

We follow Blackman and Tukey,[10] and assume that $\hat{P}(\lambda,\underline{k}_0)$ is a multiple of a chi-square variable so that to establish confidence intervals the chi-square distribution can be used with the number of degrees of freedom k given by

$$k = 2 \{E[\hat{P}(\lambda,\underline{k}_0)]\}^2 / \text{VAR}[\hat{P}(\lambda,\underline{k}_0)]$$

$$= 2M, \quad |\underline{k}_0| \neq 0$$

$$= M, \quad |\underline{k}_0| = 0.$$

24

If $M = 36$, $k = 72$ and the 90 percent confidence limits are approximately ± 1.2 db, if $\left| \underline{k}_o \right| \neq 0$. When $\left| \underline{k}_o \right| = 0$, these limits are approximately ± 1.6 db.

If the noise consists of a plane wave propagating across the array, plus incoherent noise, then, if M and N are large, the spectral matrix is given by

$$\hat{f}_{j\ell}(\lambda) = \delta_{j\ell}(R) \, \epsilon^{-i\underline{k}_o \cdot (\underline{x}_j - \underline{x}_\ell)} \, , \qquad j,\ell = 1, \ldots, K, \qquad (13)$$

where

$$\delta_{j\ell}(R) = 1 \, , \qquad j = \ell$$
$$= 1 - R, \qquad j \neq \prime \, ,$$

R is the ratio of incoherent to total noise power, $\underline{k}_o = 2\pi f \underline{\alpha}$, f is the frequency of the noise, $\underline{\alpha}$ is the slowness vector which points in the direction of propagation and has magnitude $\left| \underline{\alpha} \right| = 1/v$, v is the phase velocity of the propagating component of the noise. Hence, we have using Eq. (8)

$$\hat{P}(\lambda, \underline{k}_o) = 1 - R + \frac{R}{K}$$

The frequency-wavenumber spectrum measurement program displays contours, at a fixed frequency, of $-10 \log [\hat{P}(\lambda, \underline{k})/\hat{P}_{MAX}(\lambda, \underline{k})]$ vs $\underline{k}_x/2\pi$, $\underline{k}_y/2\pi$, where $\hat{P}_{MAX}$ is the maximum value of $\hat{P}$. The wavenumber coordinates are in cycles/km. In the present case the contours will tend to peak up at the wavenumber $\underline{k} = \underline{k}_o$, and if R is small will tend to have contours similar to those of the beam pattern $B(\underline{k})$, cf. Eq. (11).

25

We close this section by defining the sample coherence between the jth and k^{th} sensors, as used previously in the measurements on noise data,

$$\hat{C}_{jk}(\lambda) = \frac{|\hat{f}_{jk}(\lambda)|}{[\hat{f}_{jj}(\lambda)\,\hat{f}_{kk}(\lambda)]^{1/2}}$$

and the coherence is, of course,

$$C_{jk}(\lambda) = \frac{|f_{jk}(\lambda)|}{[f_{jj}(\lambda)\,f_{kk}(\lambda)]^{1/2}} \quad .$$

26

DESCRIPTION OF HIGH-RESOLUTION FREQUENCY-WAVENUMBER
SPECTRUM MEASUREMENT PROGRAM

The high-resolution estimate for $P(\lambda, \underline{k})$ is defined as

$$P'(\lambda, \underline{k}) = \left[\sum_{j,\ell=1}^{K} \hat{q}_{j\ell} \, \epsilon^{i\underline{k} \cdot (\underline{x}_j - \underline{x}_\ell)} \right]^{-1} \tag{14}$$

where $\{\hat{q}_{j\ell}(\lambda)\}$ is the inverse of the spectral matrix $\{\hat{f}_{j\ell}(\lambda)\}$. The motivation for this procedure can be given by writing Eq. (14) as

$$P'(\lambda, \underline{k}) = \sum_{j,\ell=1}^{K} A_j(\lambda, \underline{k}) \, A_\ell(\lambda, k) \, \hat{f}_{j\ell}(\lambda) \, \epsilon^{i\underline{k} \cdot (\underline{x}_j - \underline{x}_\ell)} = \frac{1}{M} \sum_{n=1}^{M} \left| \sum_{j=1}^{K} A_j(\lambda, \underline{k}) \, S_{jn}(\lambda) \right|^2 \,,$$

where

$$A_j(\lambda, \underline{k}) = \frac{\displaystyle\sum_{\ell=1}^{K} q_{j\ell}(\lambda, \underline{k})}{\displaystyle\sum_{j,\ell=1}^{K} q_{j\ell}(\lambda, \underline{k})} \tag{15}$$

and $\{q_{j\ell}(\lambda, \underline{k})\}$ is the inverse of the matrix $\{\epsilon^{i\underline{k} \cdot (\underline{x}_j - \underline{x}_\ell)} f_{j\ell}(\lambda)\}$. Thus, $P'(\lambda, \underline{k}_0)$ is the output of a maximum-likelihood filter, whose design is determined by the noise data and is different for each wavenumber $\underline{k}_0$, which passes undistorted any monochromatic plane wave travelling at a velocity corresponding to the wavenumber $\underline{k}_0$ and suppresses in an optimum manner the power of those noise waves travelling at velocities corresponding

to wavenumbers other than $\underline{k}_o$, cf. reference 14 It should be noted that the amount of computation required to obtain P' is almost the same as that to get $\hat{P}$, since only an additional Hermitian matrix inversion is required.

We now wish to compute the mean and variance of P'. In order to do this it will be assumed that the weights $A_j(\lambda, \underline{k})$ defined in Eq. (15) are not random. This is a simplifying assumption, which is not actually valid, since these weights are designed from the noise data. However, it does appear to be a reasonable approximation and the results obtained would be valid if these weights were designed somehow independent of the noise data. Using this assumption we have

$$E[P'(\lambda,\underline{k}_o)] = \int\limits_{-\pi}^{\pi} \int\limits_{-\infty}^{\infty} \int\limits_{-\infty}^{\infty} P(\lambda,\underline{k}) \, |W_N(x-\lambda)|^2 \cdot |B'(\lambda,\underline{k},\underline{k}_o)|^2 \, \frac{dx}{2\pi} \, dk_x \, dk_y \qquad (16)$$

where

$$B'(\lambda,\underline{k},\underline{k}_o) = \sum_{j=1}^{K} A_j(\lambda,\underline{k}_o) \, e^{i(\underline{k}-\underline{k}_0)\cdot\underline{x}_j} \qquad (17)$$

Thus, $E[P'(\lambda,\underline{k}_o)]$ is obtained by means of a frequency-wavenumber window $|W_N(x-\lambda)\cdot B'(\lambda,\underline{k},\underline{k}_o)|^2$. Hence, P' will be an asymptotically unbiased estimate for cP if $|W_N(x-\lambda)\cdot B'(\lambda,\underline{k},\underline{k}_o)|^2$ approaches a three-dimensional delta function in such a way that

$$\int\limits_{-\pi}^{\pi} \int\limits_{-\infty}^{\infty} \int\limits_{-\infty}^{\infty} |W_N(x-\lambda)\cdot B'(\lambda,\underline{k},\underline{k}_o)|^2 \, \frac{dx}{2\pi} \, dk_x \, dk_y = c$$

28

where c is some positive number.

The variance of P' is, assuming $\{N_{jm}\}$ is a multidimensional Gaussian process,

$$VAR[P'(\lambda,\underline{k}_o)] = \frac{1}{M}\{E[P'(\lambda,\underline{k}_o)]\}^2 + \frac{1}{M}\left|\int_{-\pi}^{\pi}\int_{-\infty}^{\infty}\int_{-\infty}^{\infty} P(\lambda,\underline{k})\,B'^*(\lambda,\underline{k},\underline{k}_o)\,B'(\lambda,\underline{k},-\underline{k}_o)\cdot\right.$$

$$\left.\cdot\,|W_N(x-\lambda)|^2\,\frac{dx}{2\pi}\,dk_x\,dk_y\right|^2$$

Thus,

$$VAR[P'(\lambda,\underline{k}_o)] \cong \frac{1}{M}\{E[P'(\lambda,\underline{k}_o)]\}^2, \quad |\underline{k}_o| \neq 0$$

$$= \frac{2}{M}\{E[P'(\lambda,\underline{k}_o)]\}^2, \quad |\underline{k}_o| = 0 .$$

The confidence limits for P' can be obtained in a manner similar to that for $\hat{P}$ described in Appendix A.

It is interesting to compute P' for the spectral matrix given in Eq. (13). If we denote this matrix by F, then

$$F = (1-R)\left[q'q + \frac{R}{1-R}\,I\right]$$

where I is the $K \times K$ identity matrix, q is a $1 \times K$ row matrix whose ij^{th} element is $\epsilon^{i\underline{k}_o\cdot\underline{x}_j}$ and q' is a $K \times 1$ column matrix whose jl^{th} element is $\epsilon^{-i\underline{k}_o\cdot\underline{x}_j}$. Now we have

$$[(1-R)(q'q + \frac{R}{1-R}I)]^{-1} = \frac{1}{R}(I - \frac{q'q}{K + \frac{R}{1-R}})$$

so that

$$P'(\lambda, \underline{k}) = \frac{R[R + K(1-R)]}{K^2[1 - R + \frac{2R}{K} - \hat{P}(\lambda, \underline{k})]}$$

Now when $\underline{k} = \underline{k}_o$, $\hat{P}(\lambda, \underline{k}_o) = 1 - R + \frac{R}{K}$ and

$$P'(\lambda, \underline{k}_o) = 1 - R + \frac{R}{K}$$

$$= \hat{P}(\lambda, \underline{k}_o)$$

The high resolution frequency-wavenumber spectrum measurement program displays contours, at a fixed frequency, of $-10 \log [P'(\lambda, \underline{k})/P'_{MAX}(\lambda, \underline{k})]$ vs $\frac{k_x}{2\pi}$, $\frac{k_y}{2\pi}$, where P'_{MAX} is the maximum value of P'. The wavenumber coordinates are in cycles/km.

It will now be shown that the wavenumber resolution using P' is higher than that of $\hat{P}$. We assume the noise is such that the spectral matrix is given by Eq. (13). In the vicinity of $\underline{k} = \underline{k}_o$ we consider the contour for which $P'(\lambda, \underline{k}) = 1 - R$, which is still very close to the peak value of $1 - R + \frac{R}{K}$, since R is small, between zero and unity, and K is large, usually about 20. For these values of $\underline{k}$ we have

$$P'(\lambda, \underline{k}) = \frac{1}{2}(1 - R + \frac{R}{K})$$

30

so that P' is already three db down from its peak value of $1 - R + \dfrac{R}{K}$. Hence, the

wavenumber resolution of P' will be much higher than that of $\hat{P}$.

We close this section by noting that the high-resolution program described is

similar to one proposed by Burg[15] and used by McCowan and Lintz.[16] Although the

two methods are different, it may be shown that both methods yield similar results.

APPENDIX C

DESCRIPTION OF COMPUTATIONS FOR OBTAINING GAIN OF BEAMFORMING AND MAXIMUM-LIKELIHOOD PROCESSING

We now wish to present a description of the computations used to obtain the results presented in Section V concerning the gain of beamforming and maximum-likelihood processing. The noise is considered to consist of two components, a component which is propagating across the array as fundamental-mode Rayleigh waves and a nonpropagating component, as described previously. The spectral matrix of the noise is computed by means of the following numerical integration over the wavenumber structure of the noise

$$f_{jk}(f) = \delta_{jk}(R) \, \epsilon^{i2\pi f \underline{\beta} \cdot (\underline{r}_j - \underline{r}_k)} \, \frac{1}{100} \sum_{n=1}^{100} \epsilon^{i2\pi f \underline{\alpha}_n \cdot \underline{r}_{jk}}$$

where $\delta_{jk}(R)$ was defined previously in Appendix A, following Eq. (13), f is the frequency in Hz, $\underline{\beta}$ is a slowness vector which points in the direction of propagation of the event, for which the array is being steered by insertion of appropriate time delays, whose magnitude is $1/V_E$, V_E is the phase velocity of the event in km/sec, $\underline{r}_j$ is the vector position of the jth sensor in km, $\underline{r}_{jk}$ is the vector position of the kth relative to the jth sensor in km, $\underline{\alpha}_n$ is a slowness vector which points outward from the origin in wavenumber space in the direction of the azimuth $\theta_N - \frac{\phi}{2} + n\frac{\phi}{100}$ and its magnitude is $1/V_N$, V_N is the phase velocity of the noise in km/sec, ϕ is the angular extent of the arc in wavenumber

32

space and θ_N is the azimuth to the center of this arc. The beamforming gain, in db, is

$$GB = -10 \log_{10} [K^{-2} \sum_{j,k=1}^{K} f_{jk}(f)]$$

The gain of maximum-likelihood processing, in db, is

$$GML = 10 \log_{10} [\sum_{j,k=1}^{K} q'_{jk}(f)]$$

where the matrix $\{q'_{jk}(f)\}$ is the inverse of $\{f_{jk}(f)\}$. The gain of ma mum-likelihood processing relative to beamforming is (GML - GB).

REFERENCES

1.   F. Press, G. Dewart and R. Gilman, "A Study of Diagnostic Techniques for Identifying Earthquakes," J. Geophys. Res., 68, May 1963.

2.   J. N. Brune, A. Espinosa and J. Oliver, "Relative Excitation of Surface Waves by Earthquakes and Underground Explosion in the California-Nevada Region," J. Geophys. Res., 68, June 1963.

3.   R. C. Liebermann, C. Y. King, J. N. Brune and P. W. Pomeroy, "Excitation of Surface Waves by the Underground Nuclear Explosion Longshot," J. Geophys. Res., 71, September 1966.

4.   P. D. Marshall, E. W. Carpenter, A. Douglas and J. B. Young, "Some Seismic Results of the Longshot Explosion," Rept. 0-67/66, Atomic Weapons Research Establishment, U. K. Atomic Energy Authority, 1966.

5.   R. C. Liebermann and P. W. Pomeroy, "Excitation of Surface Waves by Events in Southern Algeria," Science, 156, 26 May 1967.

6.   B. Gutenberg, "Amplitudes of Surface Waves and Magnitudes of Shallow Earthquakes," Bull. Seismol. Soc. Am., 35, 1945.

7.   B. Gutenberg and C. F. Richter, "Magnitude and Energy of Earthquakes," Ann. Geophys., 9, 1956.

8.   J. Capon, R. J. Greenfield and R. T. Lacoss, "Long-Period Signal Processing Results for Large Aperture Seismic Array," M. I. T., Lincoln Laboratory Technical Note 1967-50, 15 November 1967.

9.   R. A. Haubrich and G. S. MacKenzie, "Earth Noise, 5 to 500 Millicycles per Second," J. Geophys. Res., 70, 15 March 1965.

10.   R. B. Blackman and J. W. Tukey, "The Measurement of Power Spectra from the Point of View of Communication Engineering," (Dover Publications, Inc., New York: 1959).

11.   J. P. Burg, "Three-Dimensional Filtering with an Array of Seismometers," Geophysics, 29, October 1964.

12.   M. N. Toksöz and R. T. Lacoss, "Microseisms: Mode Structure and Sources,"
       Science, 15°, 1968.

13.   D. E. Amos and L. H. Koopmans, "Tables of the Distribution of the Coefficients
       of Coherence for Stationary Bivariate Gaussian Processes," Monograph SCR-483,
       Sandia Corporation, March 1963.

14.   J. Capon, R. J. Greenfield and R. J. Kolker, "Multidimensional Maximum-
       Likelihood Processing of a Large Aperture Seismic Array," Proc. IEEE, 55,
       February 1967.

15.   J. P. Burg, "An Evaluation of the Use of High-Resolution Wavenumber Spectra
       for Ambient-Noise Analysis," Texas Instruments, Inc., Special Report No. 8,
       15 February 1968.

16.   D. W. McCowan and P. R. Lintz, "High-Resolution Frequency-Wavenumber
       Spectra," Seismic Data Laboratory Report No. 206, 16 February 1968.

35
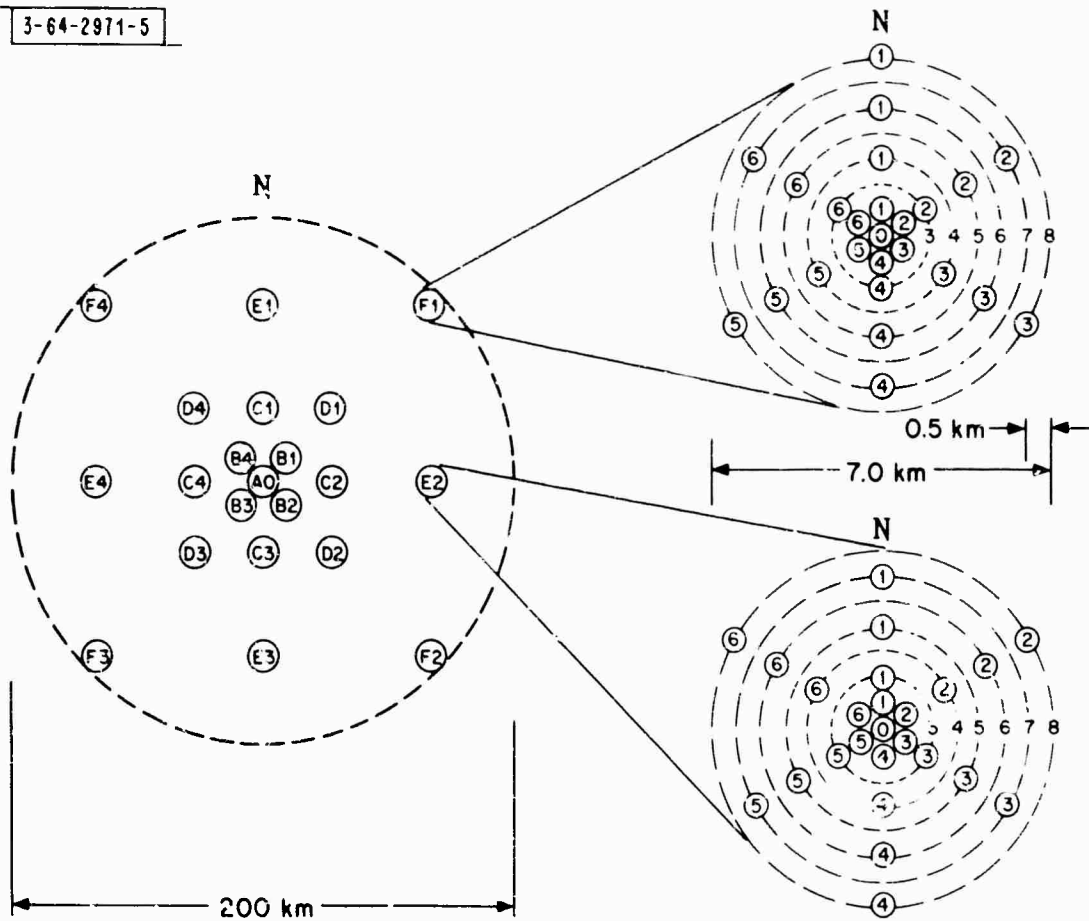
Fig. 1. General arrangement of the large aperture seismic array.
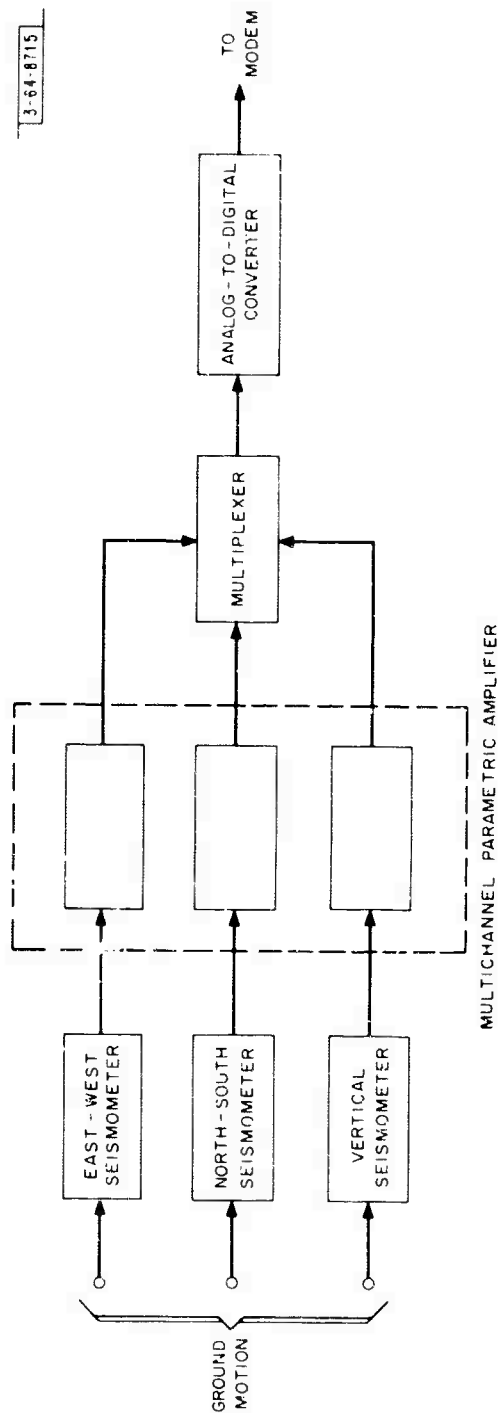
Fig. 2. Block diagram of long-period system in each subarray.

GROUND MOTION

EAST-WEST SEISMOMETER

NORTH-SOUTH SEISMOMETER

VERTICAL SEISMOMETER

MULTICHANNEL PARAMETRIC AMPLIFIER

MULTIPLEXER

ANALOG-TO-DIGITAL CONVERTER

TO MODEM
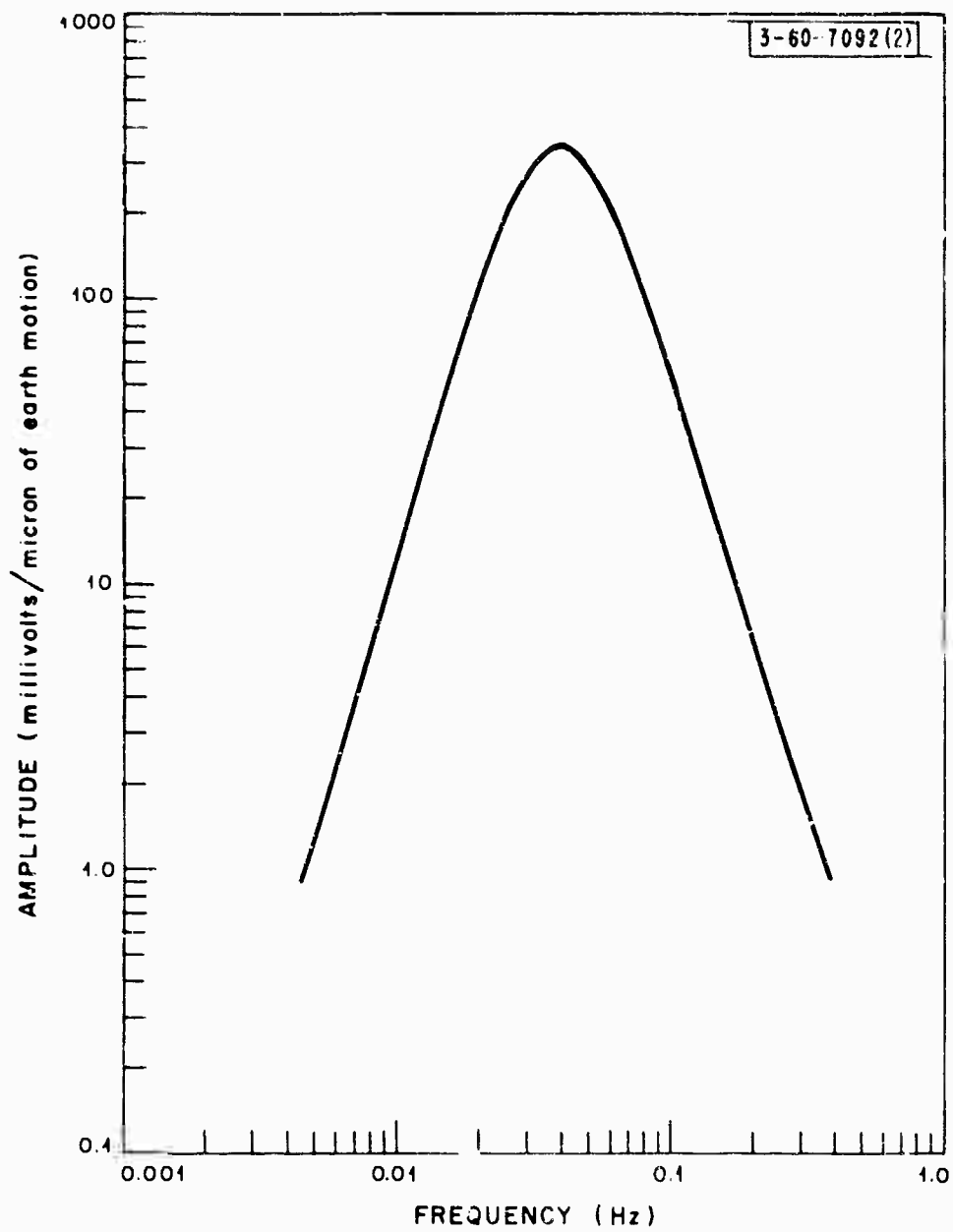
Fig. 3. Long-period system transfer function (25-second filter).
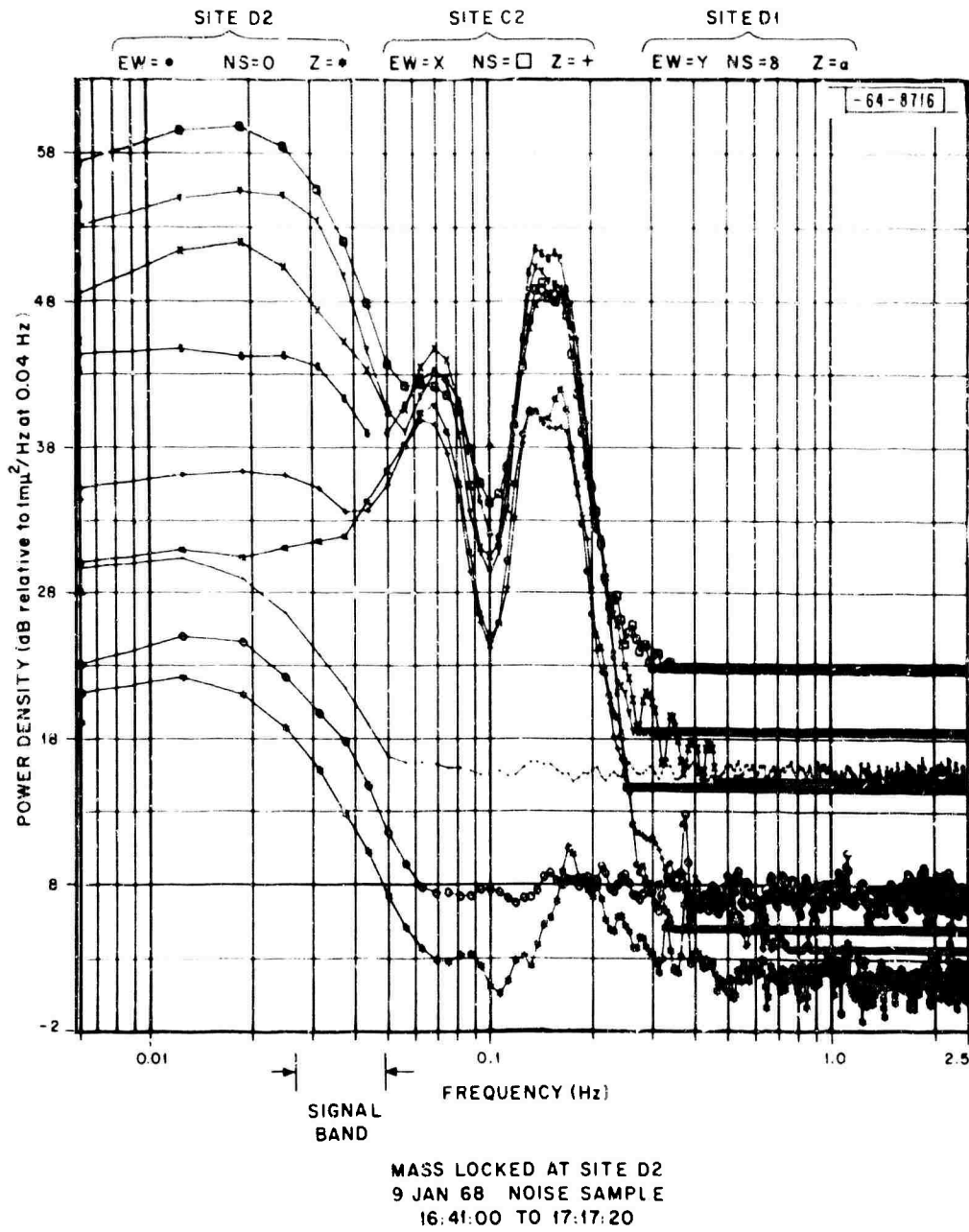
Fig. 4. Power spectral density results for locked mass test.

39
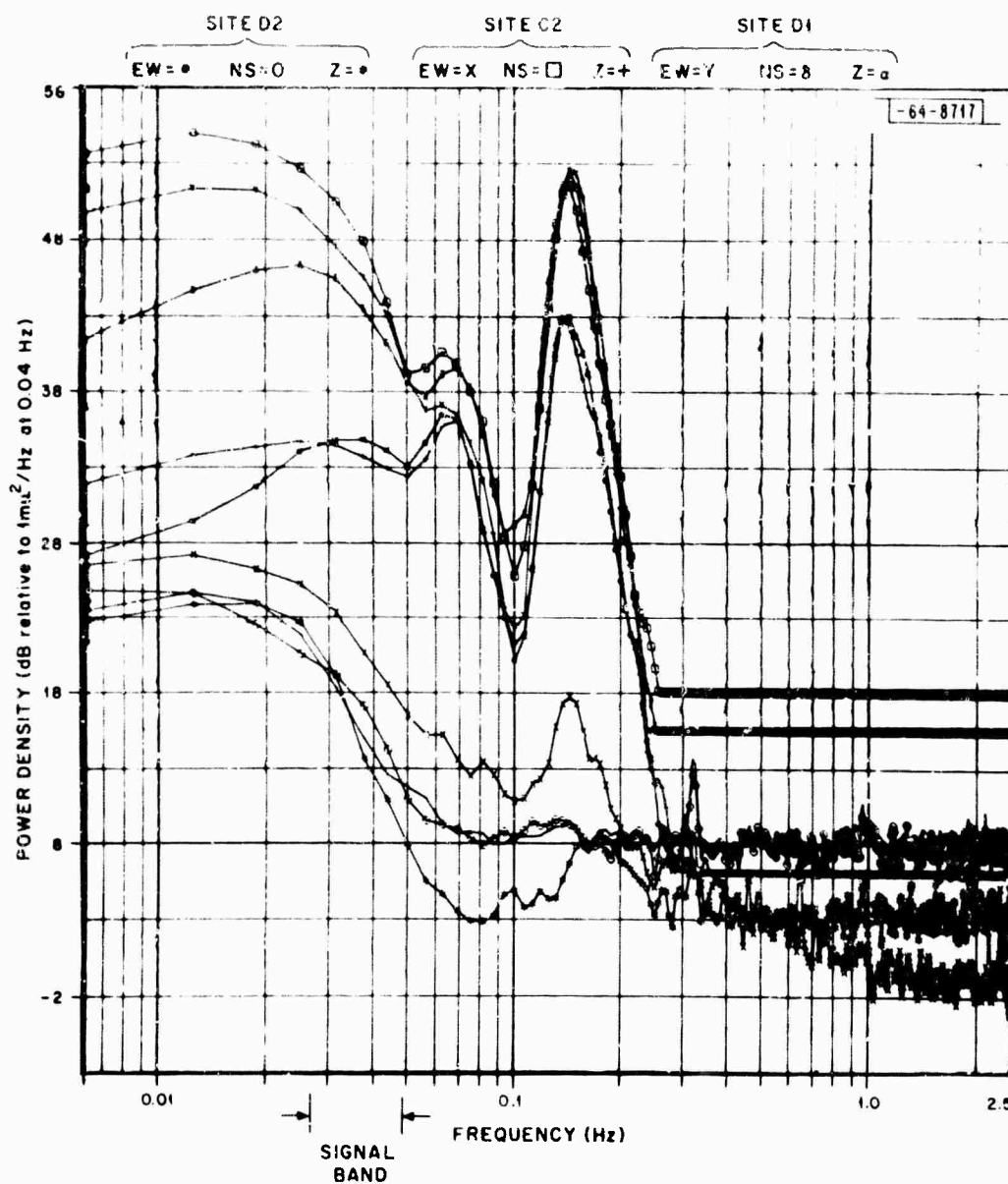
Fig. 5. Power spectral density results when seismometers at site D2 are replaced by 50 K resistance.

40
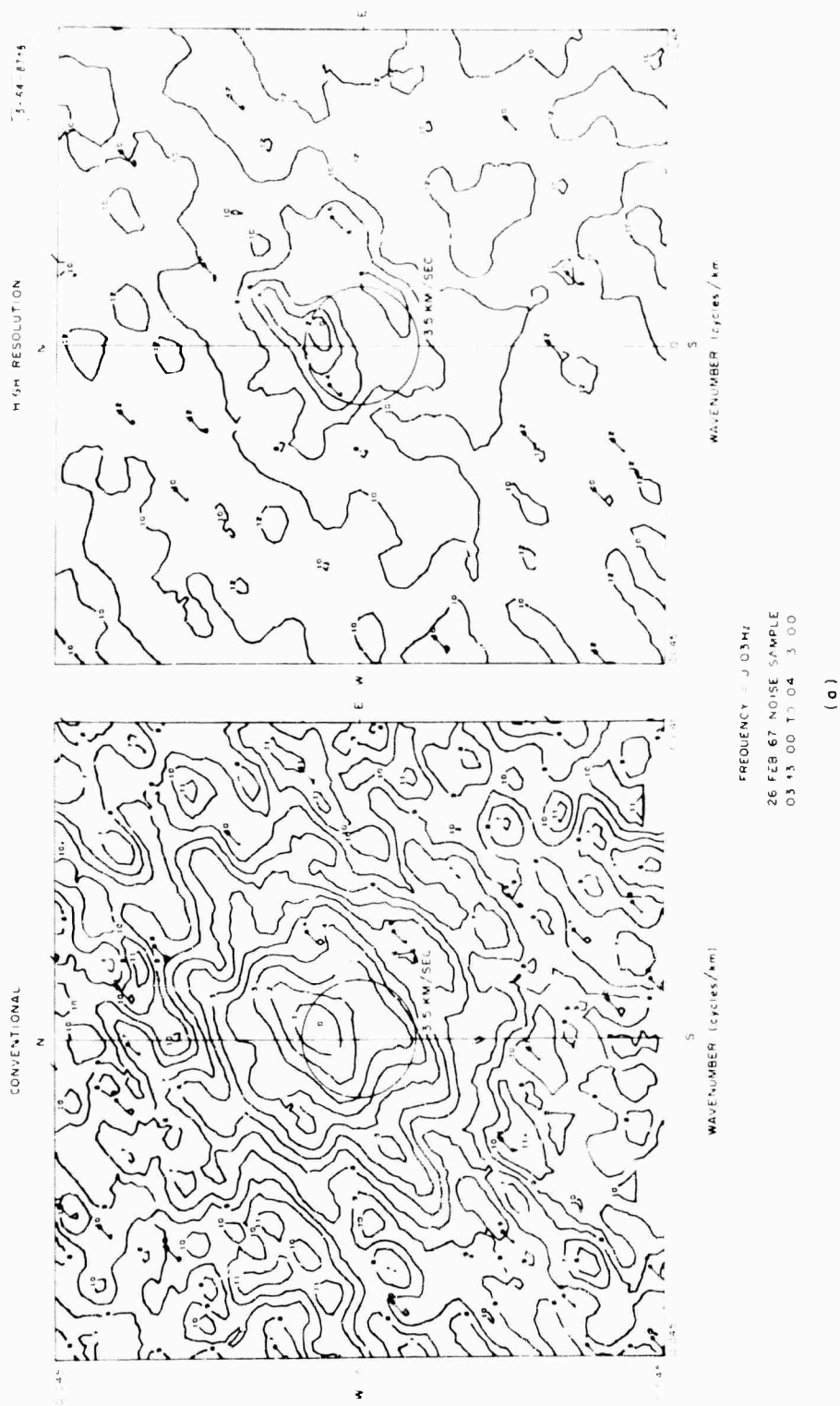
Fig. 6. Conventional and high-resolution frequency-wavenumber spectra for 26 February 1967 noise sample.

41

Fig. 6. Continued.

42

Fig. 6. Continued.

43
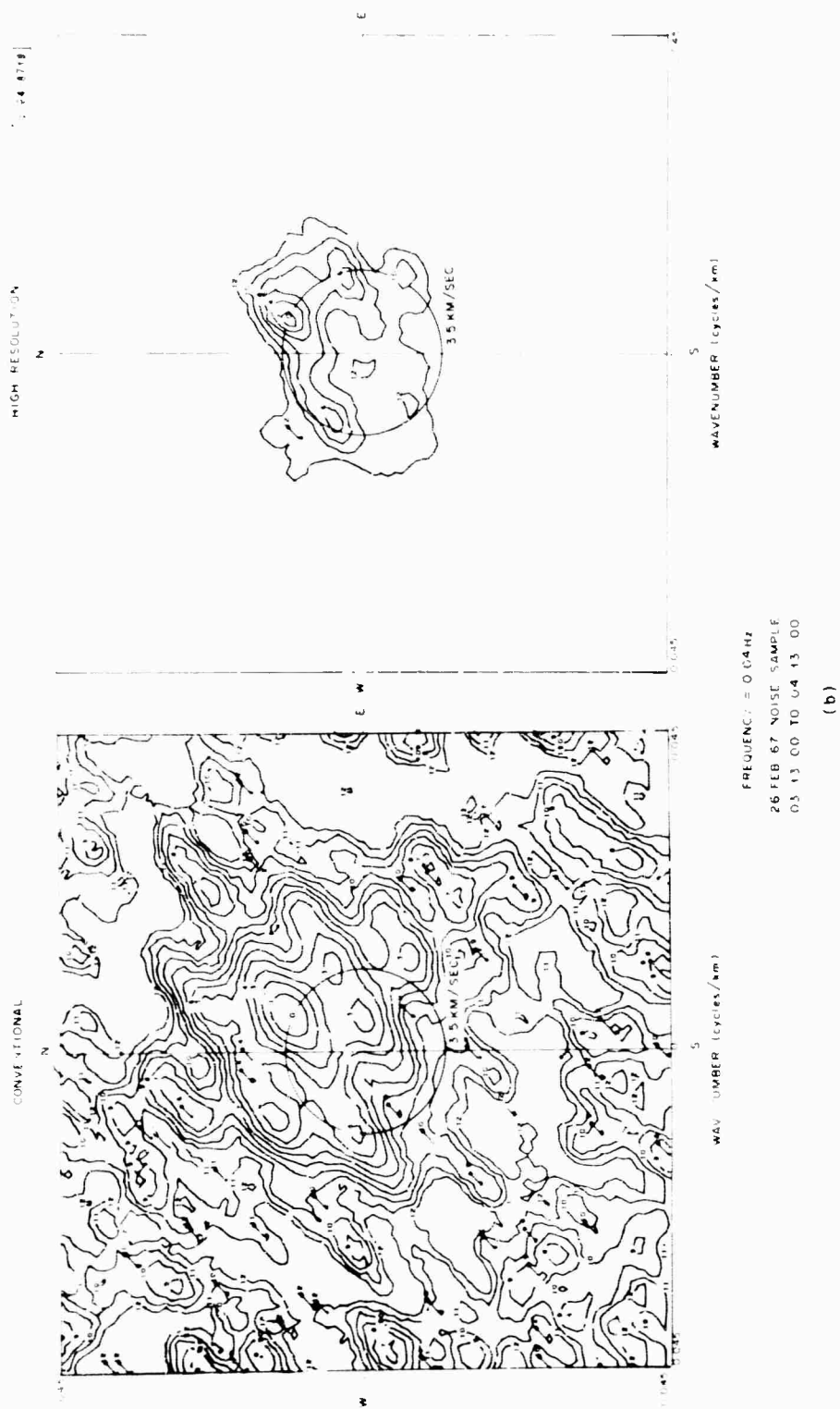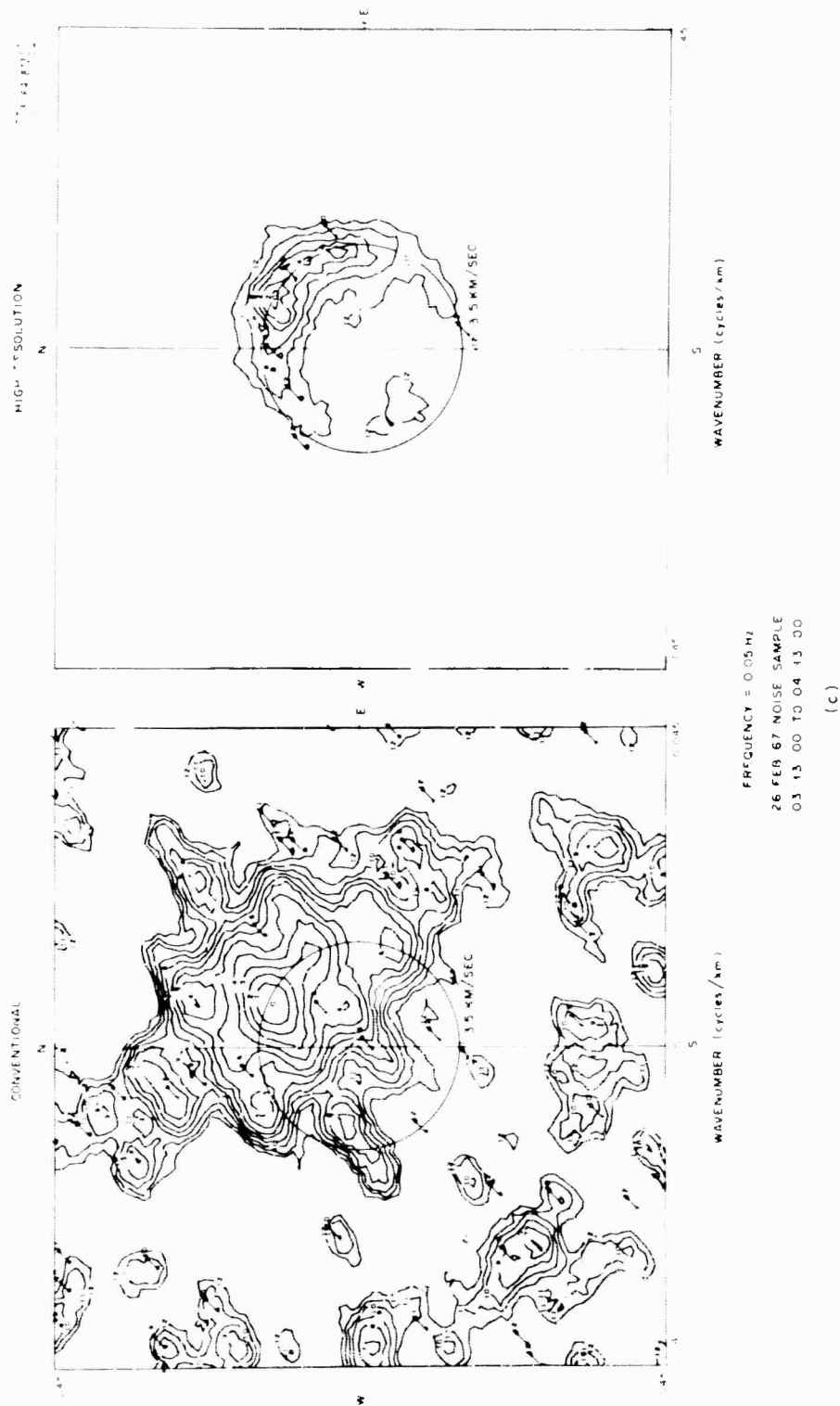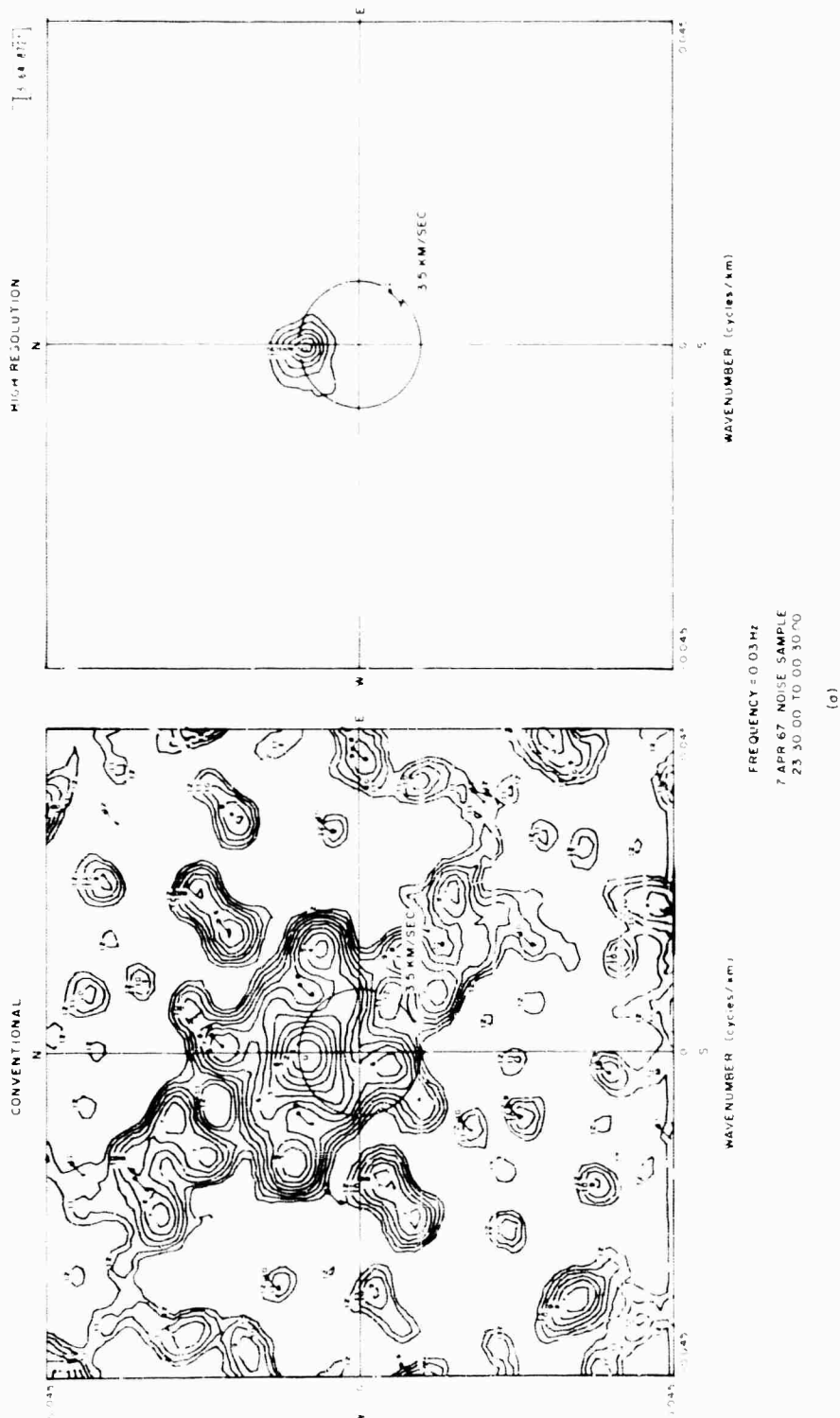
Fig. 7. Conventional and high-resolution frequency-wavenumber spectra for 7 April 1967 noise sample.

HIGH RESOLUTION

CONVENTIONAL

WAVENUMBER (cycle/km)

WAVENUMBER (cycles/km)

3 5 KM/SEC

3 5 KM/SEC
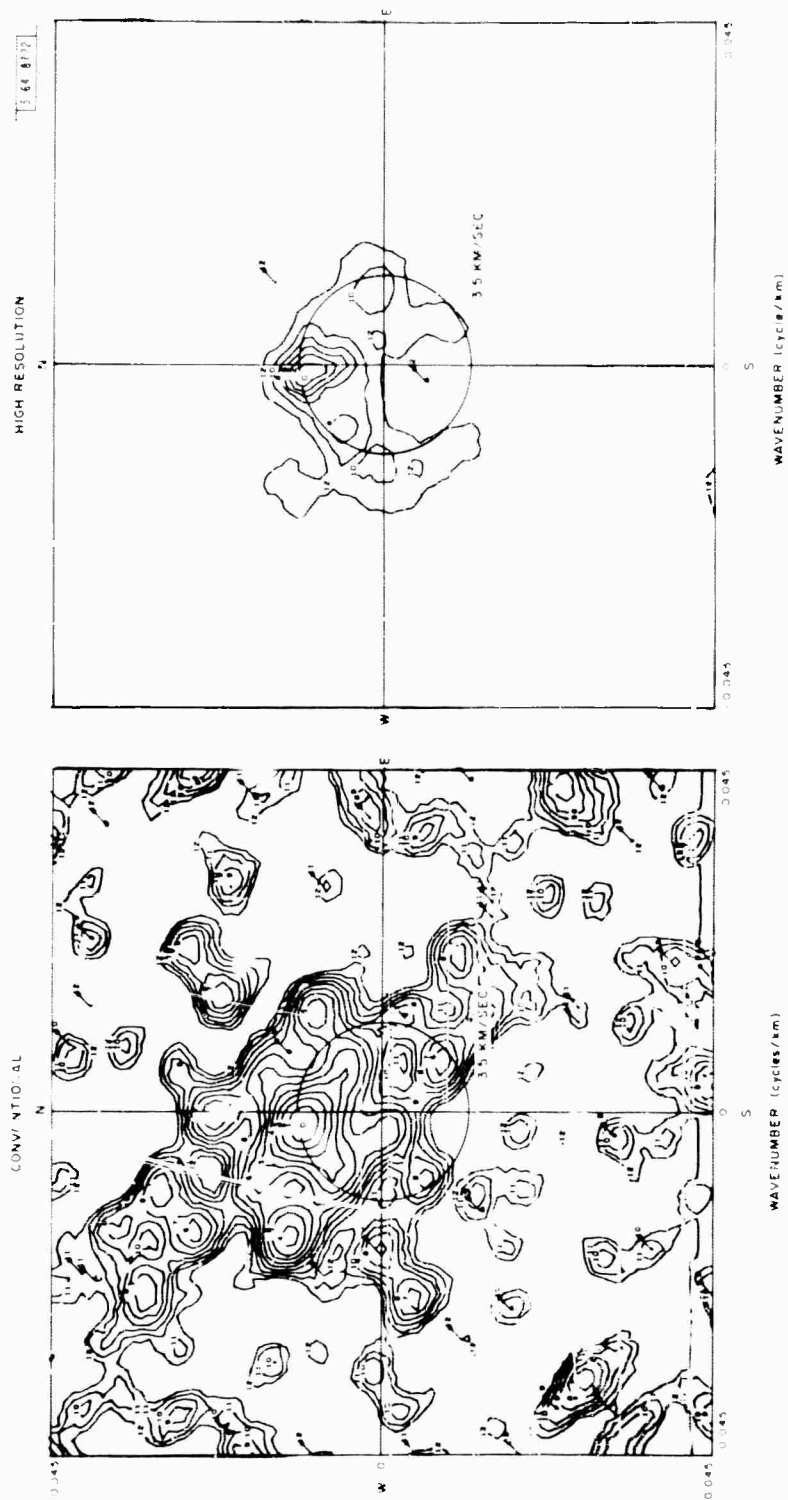
FREQUENCY = 0 04 Hz

7 APR 67 NOISE SAMPLE
23 30 00 TO 00 30 00

(b)

Fig. 7. Continued.

45

Fig. 7. Continued.

46
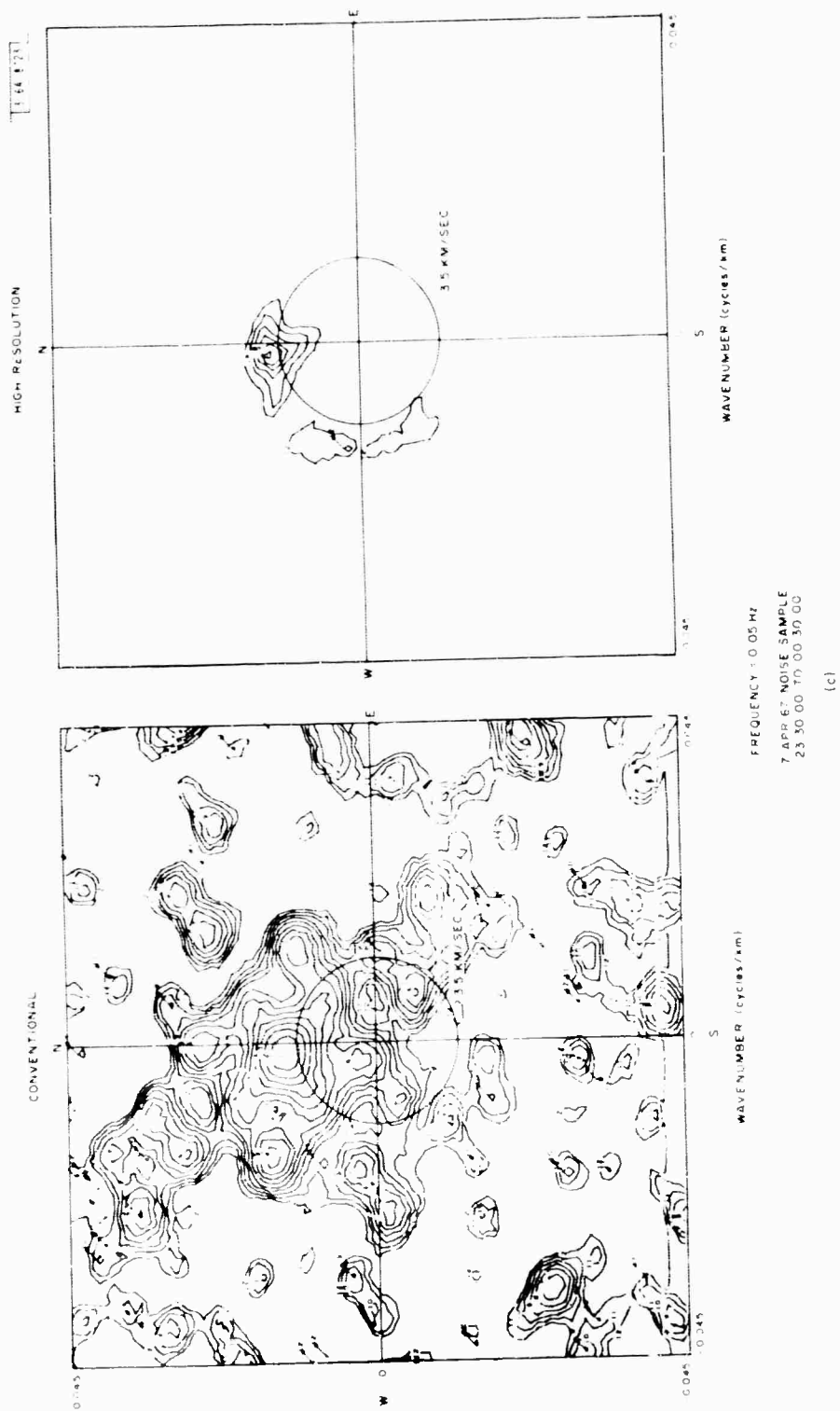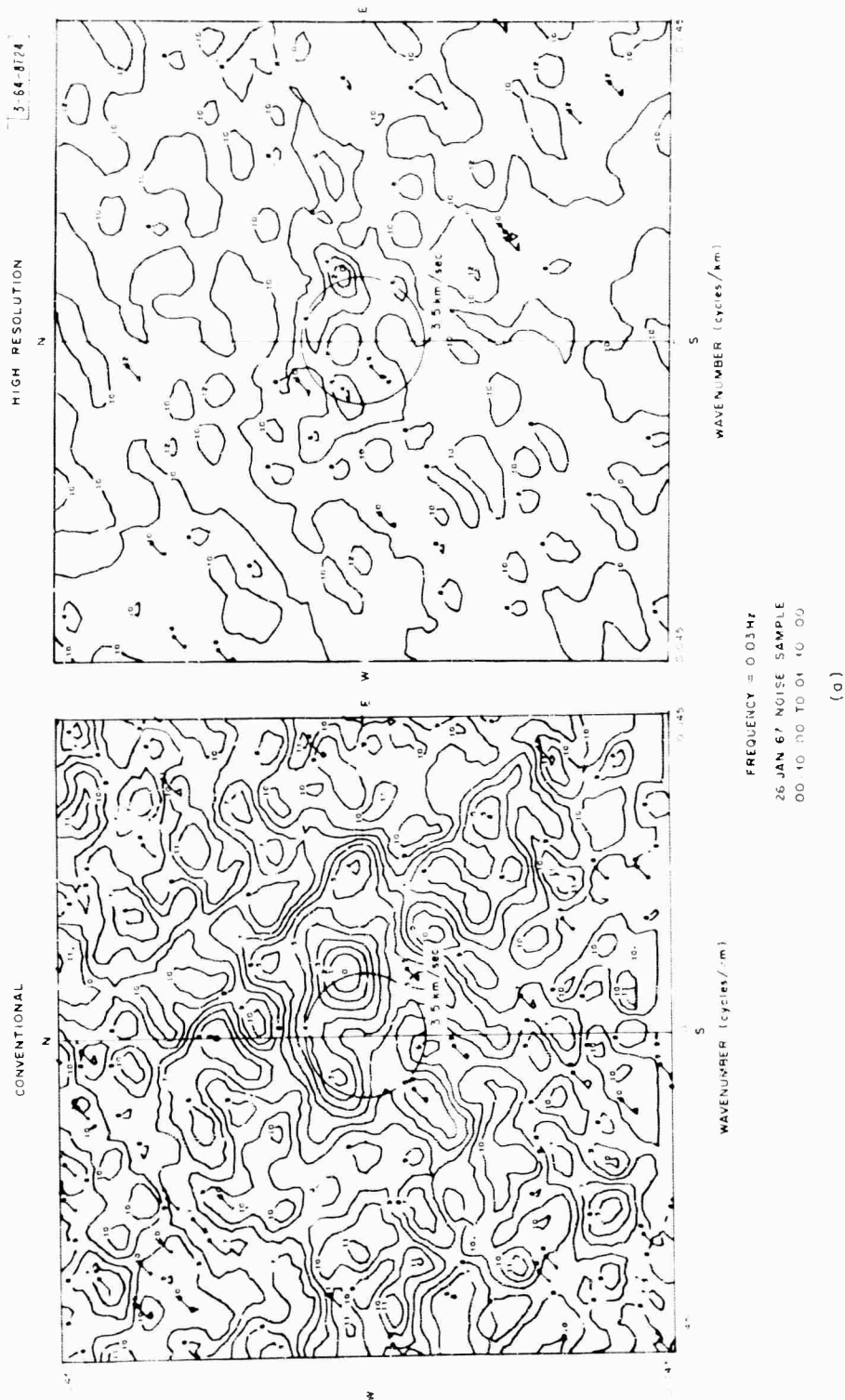
Fig. 8. Conventional and high-resolution frequency-wavenumber spectra for 26 January 1967 noise sample.

47

Fig. 8. Continued.

48

Fig. 8. Continued.

49
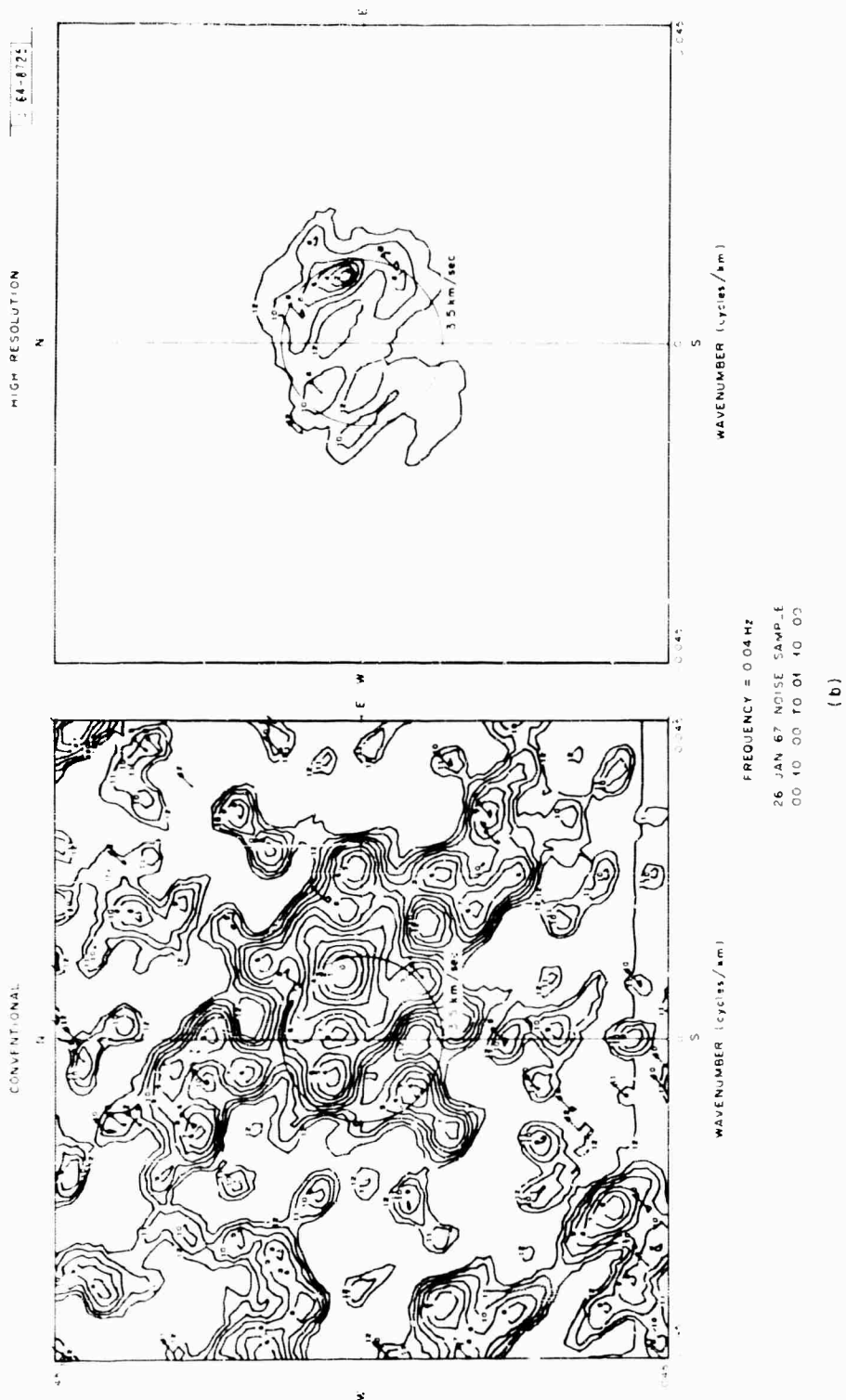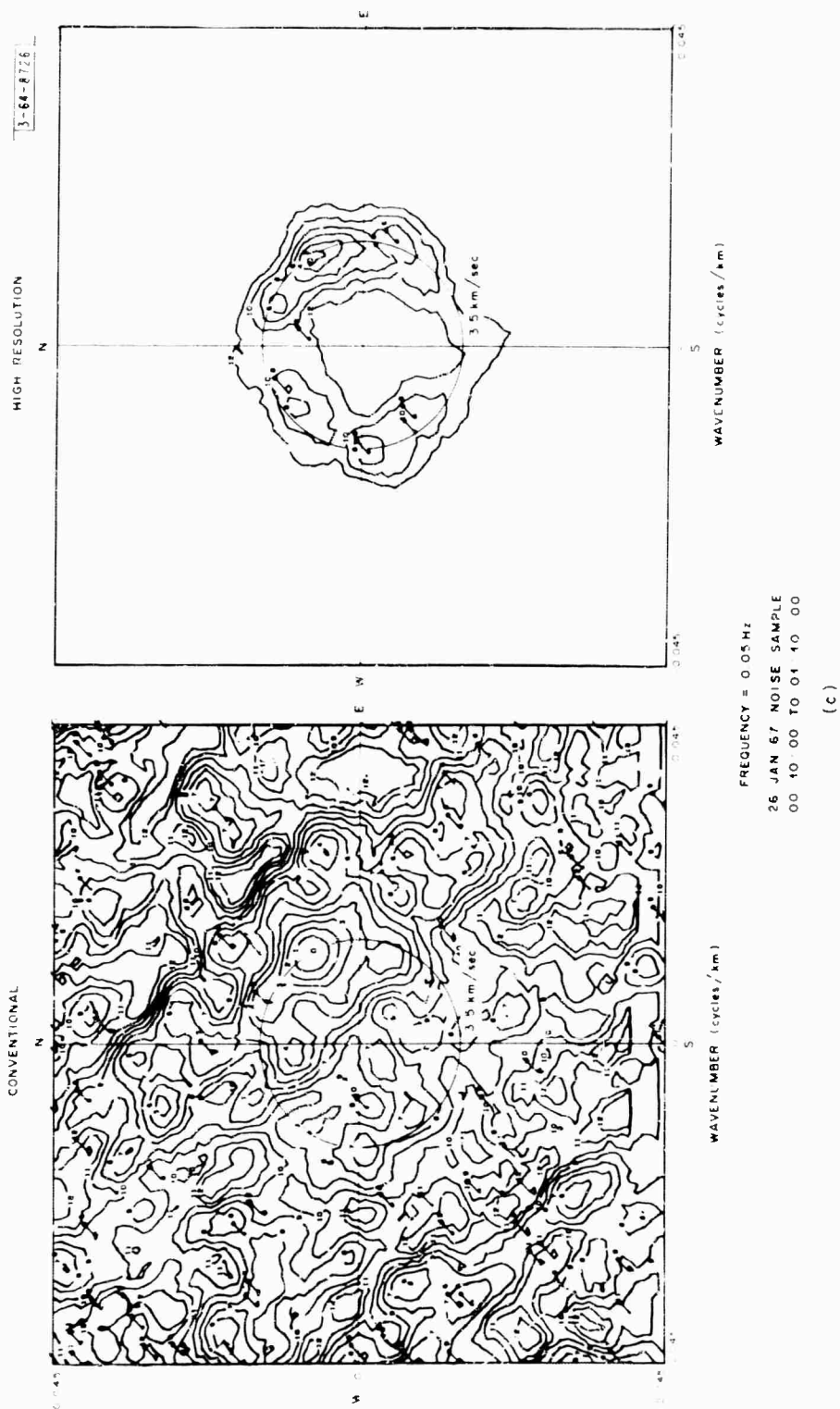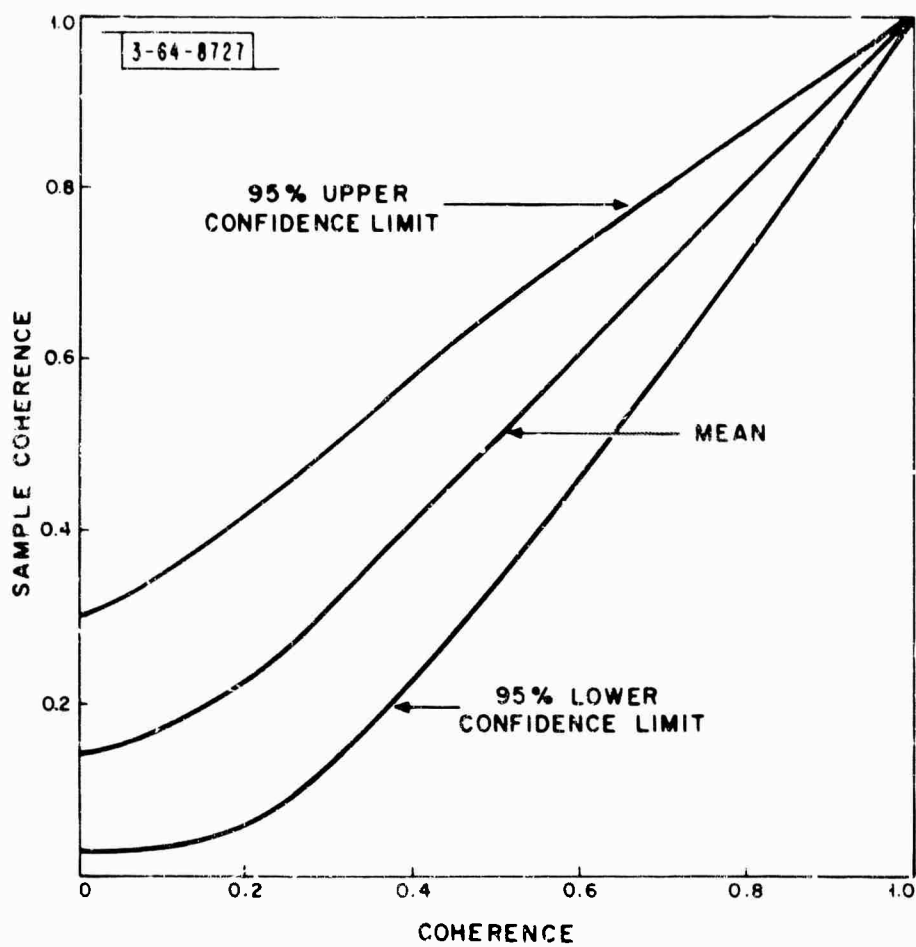
Fig. 9. The mean and 95 percent confidence limits for sample coherence using direct segment method with 36 blocks.

50
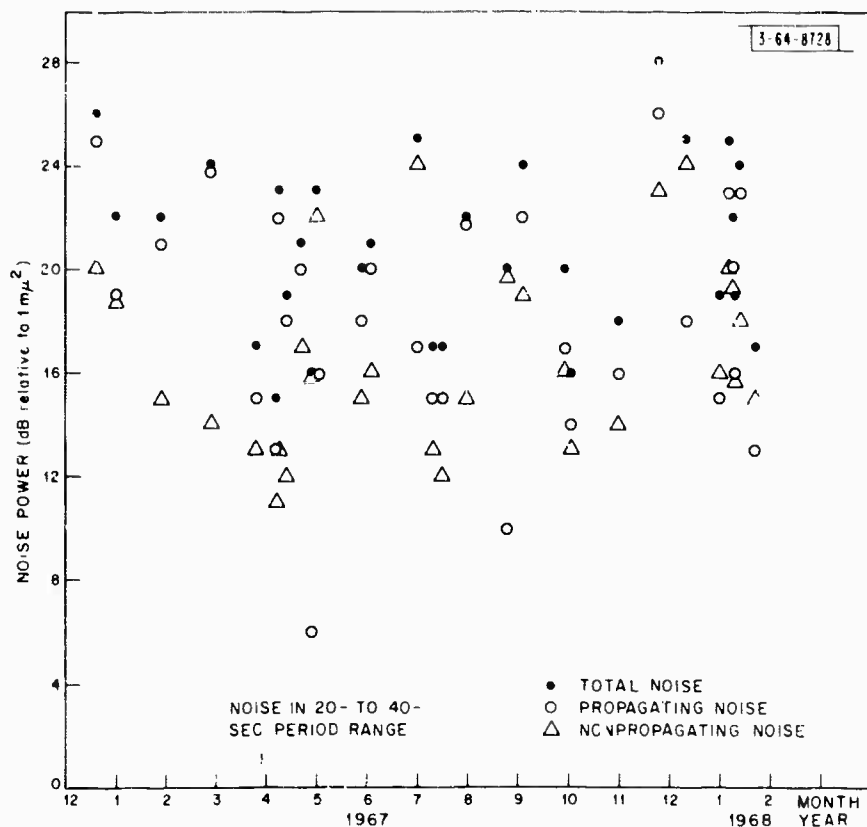
Fig. 10. Propagating, nonpropagating and total noise power in the 20 to 40 second period range vs time for 31 noise samples.

51
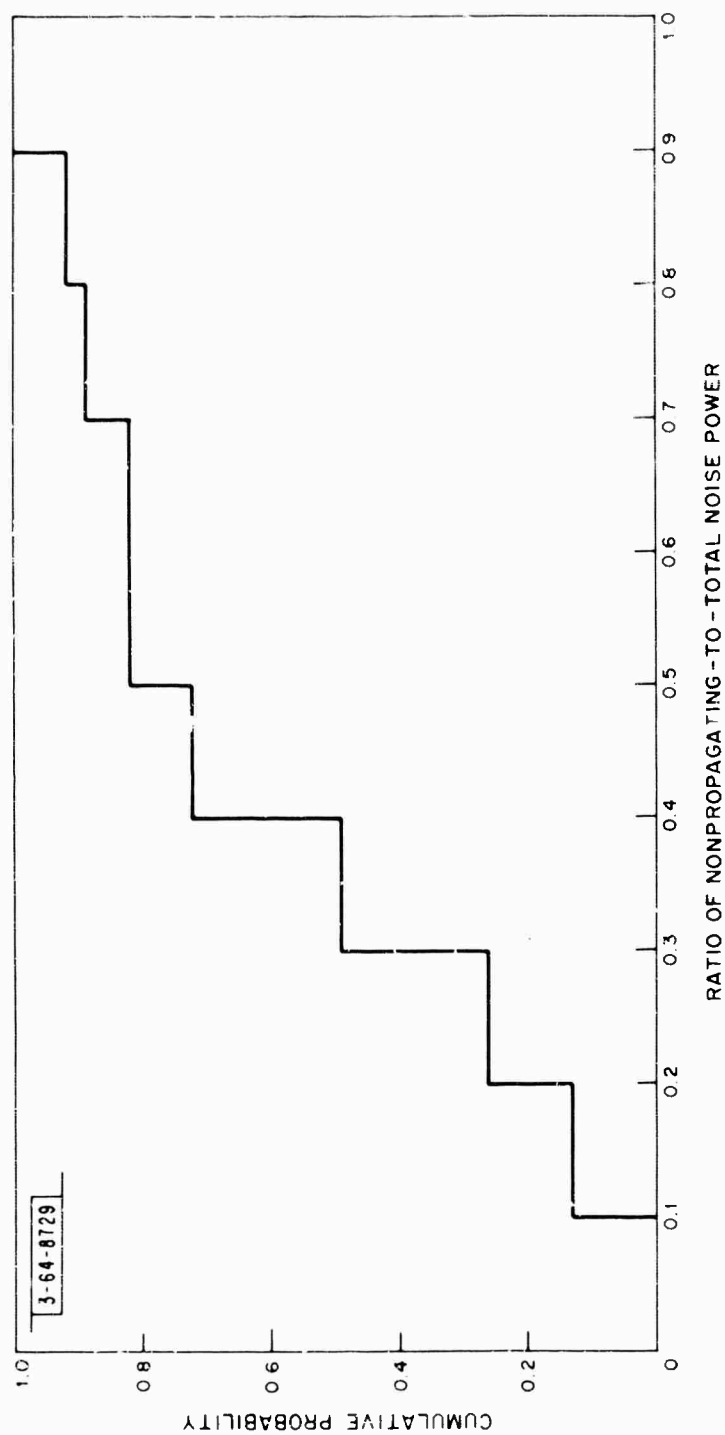
Fig. 11. Measured cumulative probability distribution function for ratio of nonpropagating to total noise power in the 20 to 40 second period range for 31 noise samples.

52
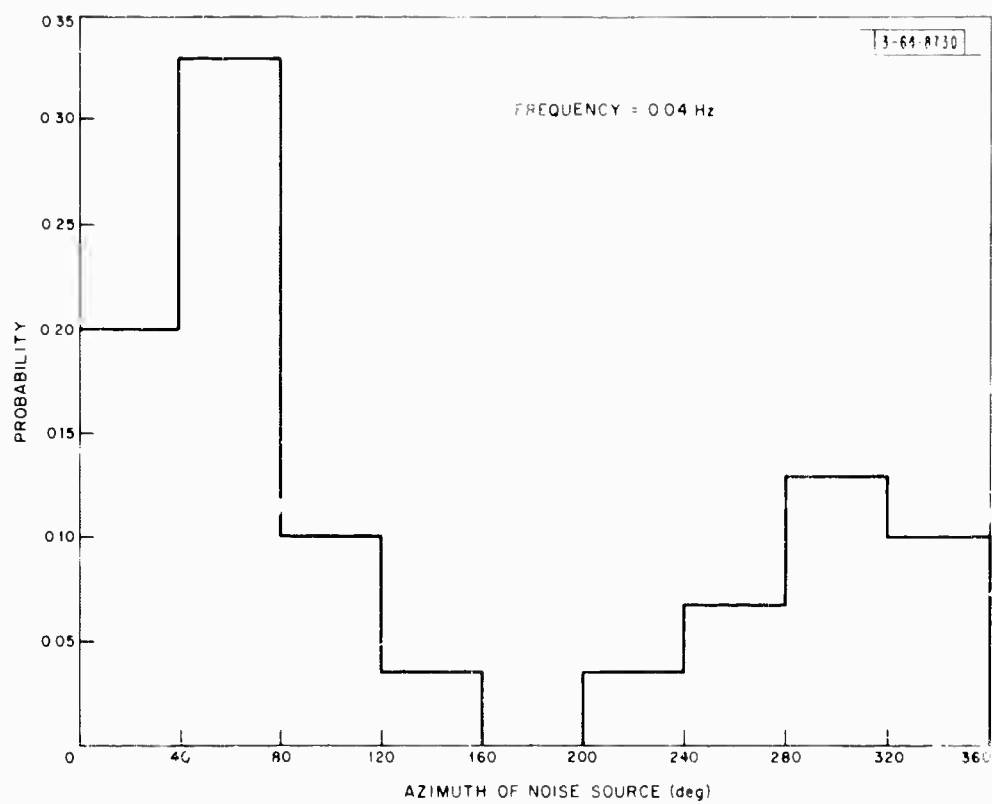
Fig. 12.   Histogram of noise-source azimuths observed at the large aperture seismic array at 25 second period for 31 noise samples.
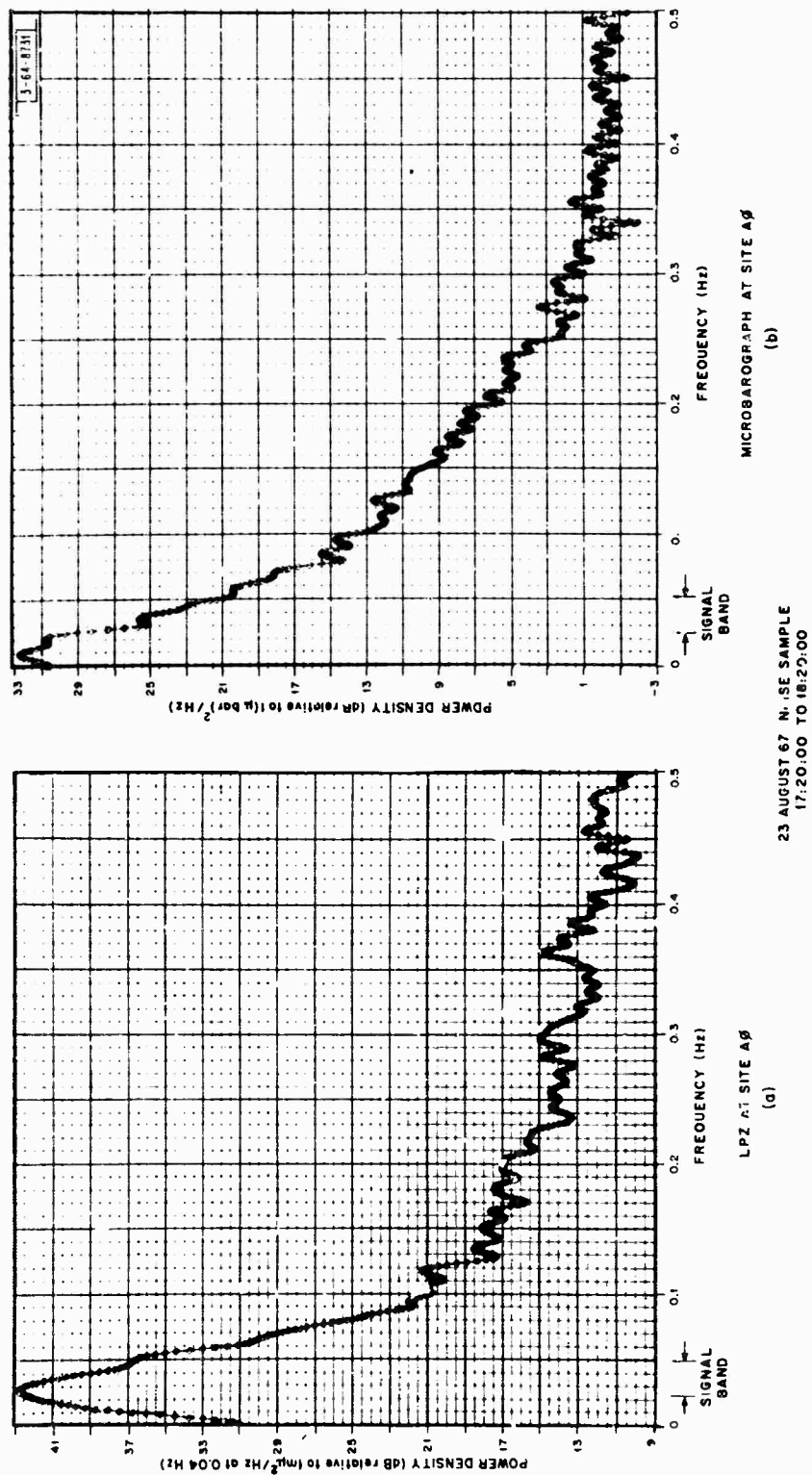
Fig. 13. Power spectral densities for long-period seismic noise and microbarograph record at site AØ.
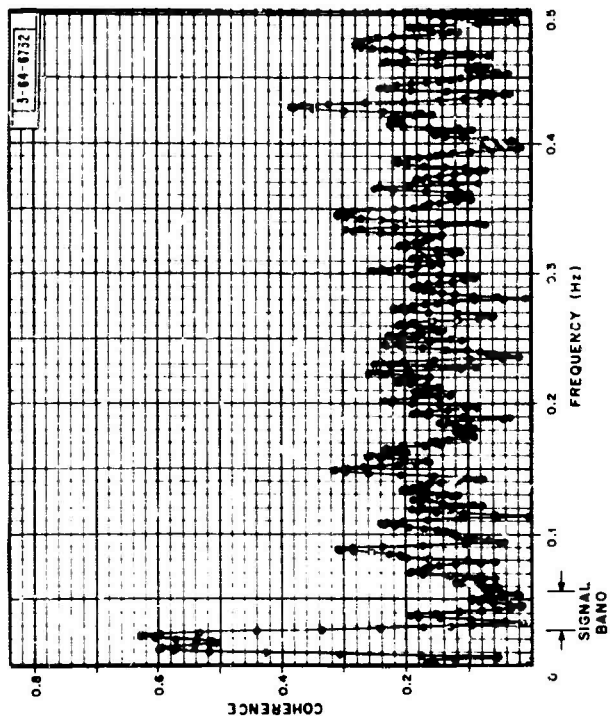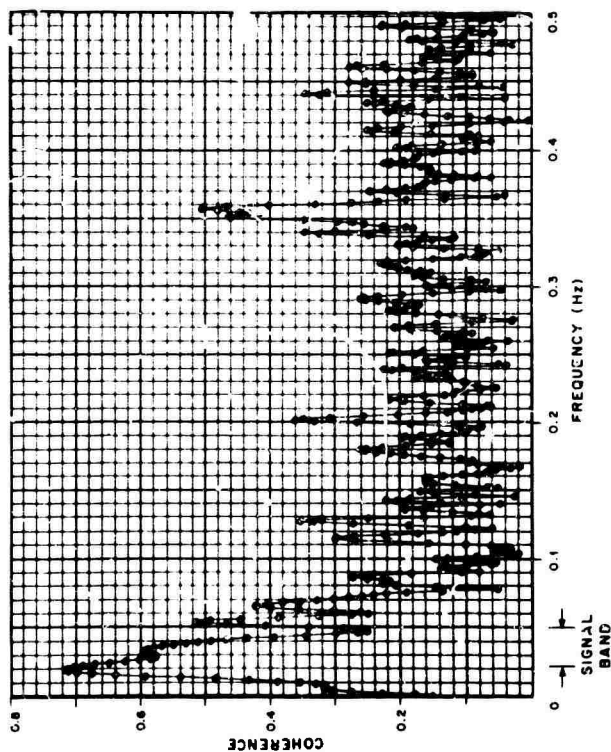
Fig. 14. Coherence between long-period vertical seismometer and microbarograph, at site AØ, for two noise samples.
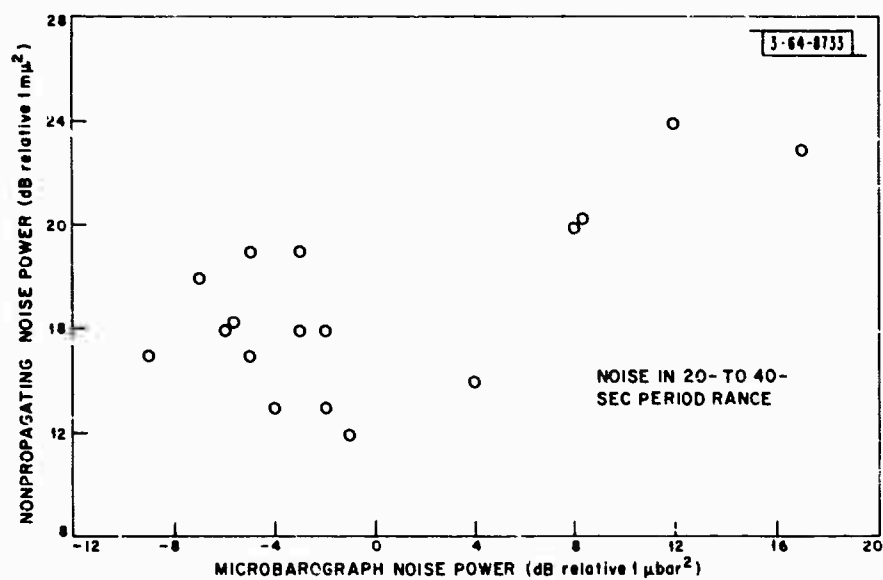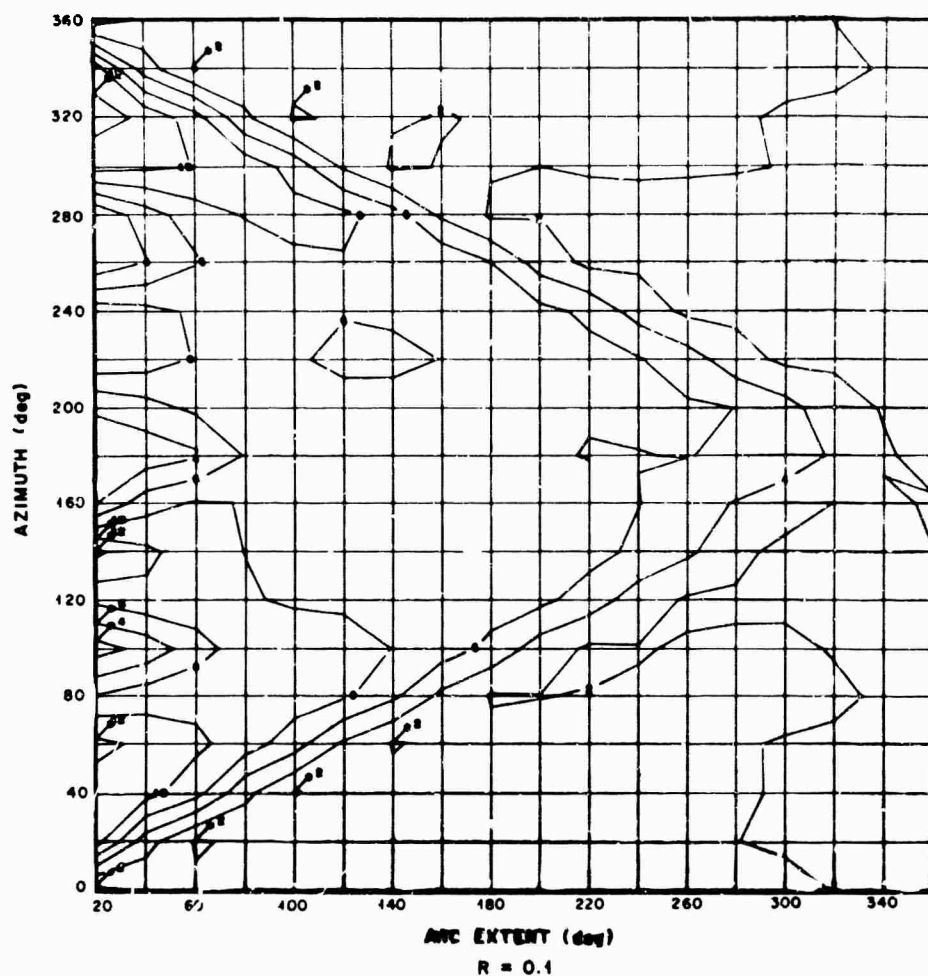
55

Fig. 15. Nonpropagating seismic noise power vs microbarograph noise power in the 20 to 40 second period range, at site A∅.
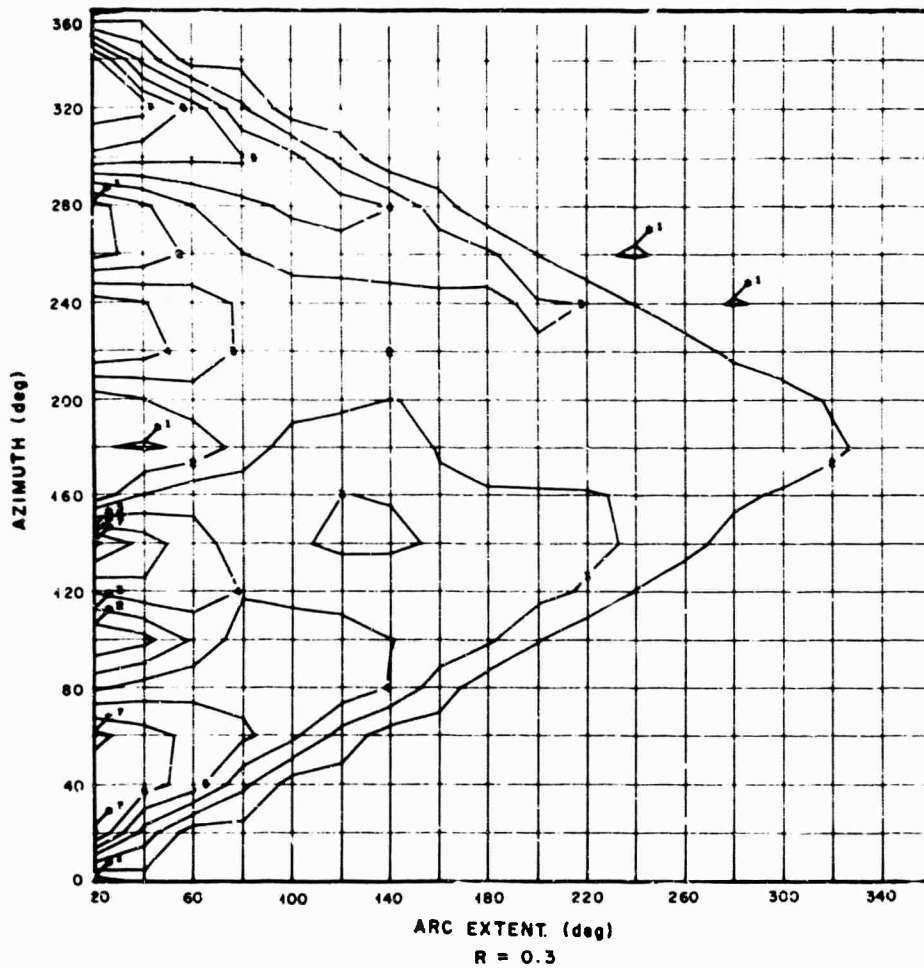
R = RATIO OF NONPROPAGATING - TO - TOTAL NOISE POWER
AZIMUTH OF EVENT = 0 DEG
VELOCITY OF EVENT AND NOISE = 3 7 KM/SEC
FREQUENCY = 0.04 Hz

(a)

Fig. 16. Gain of maximum-likelihood processing relative to beamforming.

R = RATIO OF NONPROPAGATING - TO - TOTAL NOISE POWER

AZIMUTH OF EVENT = O OEG

VELOCITY OF EVENT AND NOISE = 3.7 KM/SEC
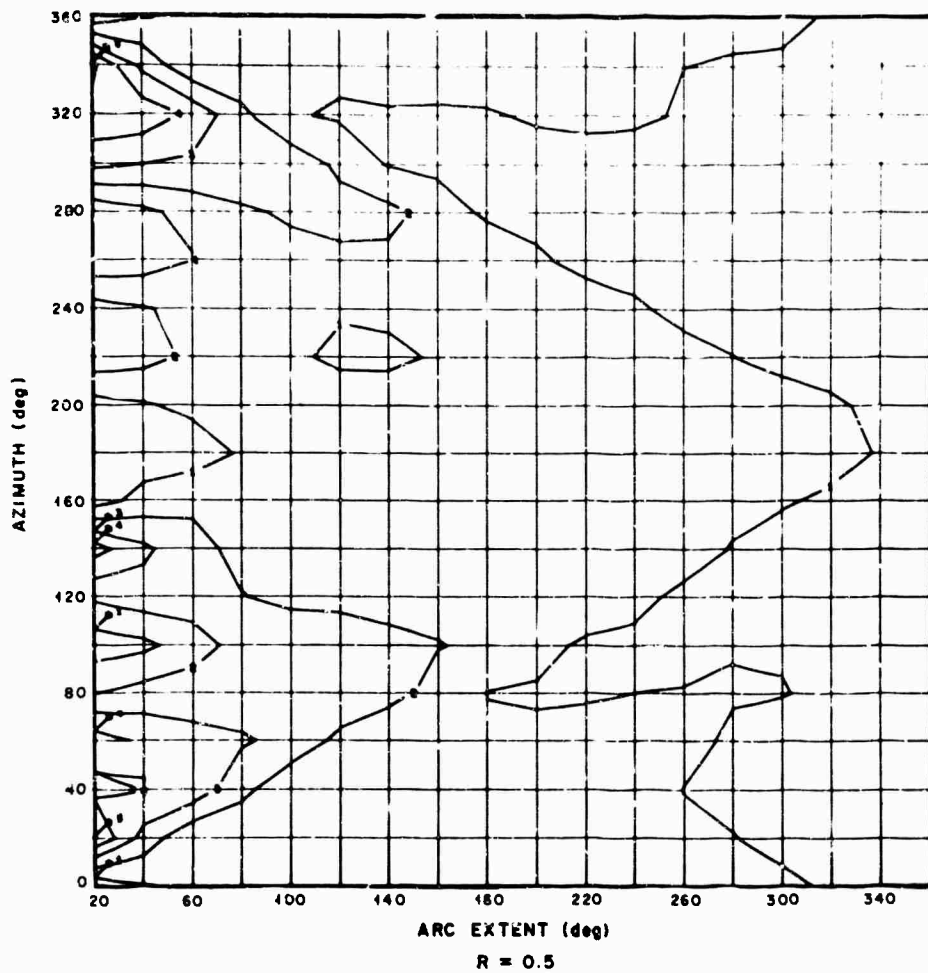
FREQUENCY = 0.04 Hz

(b)

Fig. 16. Continued.

58

R = RATIO OF NONPROPAGATING-TO-TOTAL NOISE POWER
AZIMUTH OF EVENT = 0 DEG
VELOCITY OF EVENT AND NOISE = 3.7 KM/SEC
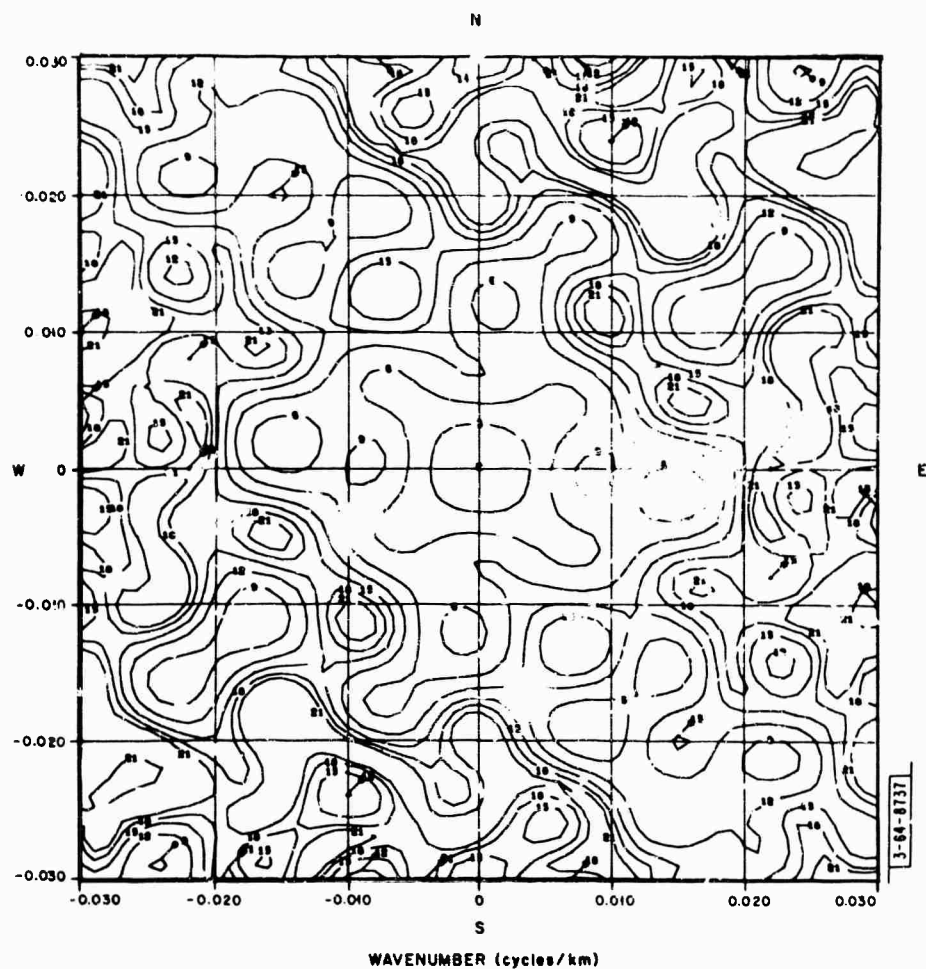FREQUENCY = 0.04 Hz

(c)

Fig. 16.   Continued.

Fig. 17.   The beamforming array response pattern for the large aperture seismic array.

DOCUMENT CONTROL DATA - R&D

(Security classification of title, body of abstract and indexing annotation must be entered when the overall report is classified)

1. ORIGINATING ACTIVITY (Corporate author)	2a. REPORT SECURITY CLASSIFICATION
Lincoln Laboratory, M.I.T.	Unclassified
	2b. GROUP None

3. REPORT TITLE

Investigation of Long Period Noise at LASA

4. DESCRIPTIVE NOTES *(Type of report and inclusive dates)*

Technical Note

5. AUTHOR(S) *(Last name, first name, initial)*

Capon, Jack

6. REPORT DATE	7a. TOTAL NO. OF PAGES	7b. NO. OF REFS
3 June 1968	66	16

8a. CONTRACT OR GRANT NO. AF 19(628)-5167	9a. ORIGINATOR'S REPORT NUMBER(S)
b. PROJECT NO. ARPA Order 512	Technical Note 1968-15
c.	9b. OTHER REPORT NO(S) *(Any other numbers that may be assigned this report)*
d.	ESD-TR-68-176

10. AVAILABILITY/LIMITATION NOTICES

This document has been approved for public release and sale; its distribution is unlimited.

11. SUPPLEMENTARY NOTES	12. SPONSORING MILITARY ACTIVITY
None	Advanced Research Projects Agency, Department of Defense

13. ABSTRACT

The long-period noise in the 20 to 40 second period range limits the identification level at which the surface-wave, body-wave discriminant can be applied at the Large Aperture Seismic Array (LASA). Therefore, an investigation was made to determine the sources and properties of this noise. Only the long-period vertical array at LASA was considered.

Both conventional and high-resolution frequency-wavenumber spectra are presented for the noise, as well as coherence results. These data show that the noise consists of two components. One component propagates across the array as fundamental-mode Rayleigh waves and is known to be caused by the action of surf on coastlines. The other component is nonpropagating and evidence is presented which indicates it is caused by the elastic loading on the ground by the earth's atmosphere. This is established by correlating the power of the nonpropagating noise with the power on the microbarograph sensors at LASA.

It is also shown that the signal-to-noise ratio gain obtained with maximum-likelihood processing relative to that obtained with beamforming for the long-period noise present at LASA, will not be substantial unless it can be shown that significant amounts of propagating noise power, relative to total noise power, are present. The results at LASA indicate that such large amounts of propagating noise power are rarely to be observed.

14. KEY WORDS

LASA   long period noise seismic noise
noise